STUDY OF PHYSICAL PROPERTIES OF MAX PHASES M_2TlC (M = Ti, Zr, Hf): A DFT CALCULATION

By

Mohammed Sohel

Student ID: 15MPHY004P

A thesis submitted in partial fulfilment of the requirements for the degree of

MASTER of PHILOSOPHY

Department of Physics

CHITTAGONG UNIVERSITY OF ENGINEERING & TECHNOLOGY

August 2023

Declaration

I hereby declare that the work contained in this thesis has not been previously submitted to meet requirements for an award at this or any other higher education institution. To the best of my knowledge and belief, the Thesis contains no material previously published or written by another person except where due reference is cited. Furthermore, the Thesis complies with PLAGIARISM and ACADEMIC INTEGRITY regulation of CUET.

Mohammed Sohel
Student ID: 15MPHY004P
Department of Physics
Chittagong University of Engineering & Technology (CUET)

Dedication

To my beloved Father & Mother infinitely supportive

List of Publications

Journal Article

- Publication: M. Sohel, M. M. Uddin, M. A. Ali, M. M. Hossain, A. K. M. A. Islam and S. H. Naqib, "Impact of M atomic species on physical properties of M_2TlC (M= Ti, Zr, Hf): a first principle calculation", **AIP Advances 13, 065209 (2023),** https://doi.org/10.1063/5.0150252

Conference

- M. Sohel, M. A. Ali, M. M. Hossain, S. H. Naqib, A. K. M. A. Islam and M. M. Uddin, "Influence of M atomic species on physical properties of MAX phases M_2TlC (M= Ti, Zr, Hf): a DFT calculations", Poster presentation, Intern*ational Conference on Physics*, 19-21 May, 2022, Organized by Bangladesh Physical Society (BPS) at AECD, Dhaka, Bangladesh.

Approval/Declaration by the Supervisor(s)

This is to certify that Mohammed Sohel has carried out this research work under my supervision, and that he has fulfilled the relevant Academic Ordinance of the Chittagong University of Engineering and Technology, so that he is qualified to submit the following Thesis in the application for the degree of MASTER of PHILOSOPHY IN PHYSICS. Furthermore, the Thesis complies with the PLAGIARISM and ACADEMIC INTEGRITY regulation of CUET.

Dr. Md. Mohi Uddin
Professor
Department of Physics
Chittagong University of Engineering & Technology

Acknowledgement

First and foremost, I would like to thank the Almighty for giving me the strength, knowledge, ability and opportunity to undertake this research study and complete it satisfactorily.

I am grateful to the authority of Chittagong University of Engineering & Technology (CUET) for all kind of support.

I am deeply indebted to my supervisor Prof. Dr. Md. Mohi Uddin, Department of Physics, CUET. He guided me all the way with his characteristic wisdom and patience and bore all my limitations with utmost affection.

I want to express my sincere gratitude to Prof. Dr. Md. Ashraf Ali and Dr. Md. Mukter Hossain, Associate Professor, Department of Physics, CUET for cordial inspiration and suggestions during the progress at each step of this work.

I am grateful to my respectable teacher Prof. Dr. Faruque-Uz-Zaman Chowdhury, Prof. Dr. Mohammad Belal Hossen, Prof. Dr. Swapan Kumar Roy, Prof. Dr. H.M.A.R. Maruf, Prof. Dr. Nusrat Jahan, Prof. Dr. Animesh Kumar Chakarborty, Md. Abdul Jalil of Department of Physics, CUET who provided very useful guidance along the way.

Finally, I wish to express my gratitude to my parents, parents-in-laws and spouse had been very patient and understanding and made great sacrifices during the whole course of this study.

Abstract

The projected ternary carbide MAX phases M_2TlC (M = Ti, Zr, and Hf) have been investigated for their phonon dispersion and optical properties, including Mulliken population analysis, optical and theoretical Vickers hardness. We reviewed the compound's structural and electrical characteristics to evaluate the accuracy of our calculations. The examined MAX phases are mechanically and dynamically stable, according to the examination of the formation energies, elastic constants, phonon dispersion, and phonon density of states. Ti-3d, Zr-4d, Hf-5p, 5d, and Tl-6p electronic orbitals, which have a substantial impact on the phases' physical characteristics and heavily contribute to electronic conduction, are the main causes of the sub-band crossing the E_F. For the phases, the values of total density of states (TDOS) at E_F are determined to be 3.0, 2.55, and 2.09 states/eV. In the compounds under investigation, the bond Hf-C has the highest covalency of all the bonds. The hardness of the examined compounds may be compared in such a way that Ti_2TlC for both H_{micro} (24 GPa) and H_{macro} (17 GPa) is harder than that of Hf_2TlC (17 and 13 GPa) and Zr_2TlC (20 and 16 GPa). The Vickers hardness are discovered to be 2.18, 1.61, and 2.60 GPa, respectively for the phases. The reported hardness values are in the range of 2 to 8 GPa that is comparable with the well-known MAX phase nanolaminates, such as Hf_2InC (3.45 GPa) and Ta_2InC (4.12 GPa). The values of the longitudinal optical (LO) and transverse optical (TO) components at Γ are 19.74 and 21.63 THz (Ti_2TlC), 16.62 and 17.18 THz (Zr_2TlC), and 18.66 and 19.94 THz (Hf_2TlC), respectively. The phonon dispersion curves (across the entire BZ) do not exhibit imaginary (negative on the frequency scale) phonon frequency, suggesting the dynamic stability of the phases. The value of reflectivity rises to high as 92%, 82%, and 86% for the compounds Ti_2TlC, Zr_2TlC, and Hf_2TlC, respectively, at energy 8.76 eV, 9.6 eV, and 10.7 eV. It is an intriguing observation that the reflectivity is always greater than 44% for the phases Ti_2TlC (11.67 eV), Zr_2TlC (12.44 eV), and Hf_2TlC (13.8 eV). According to reflectivity's findings, the visible (1.7 eV–3.3 eV) and IR (1.24 eV–1.7 eV) sectors account for more than 44% of the energy up to 12.0 eV. Therefore, the investigated compounds might be a good contender for use as a covering material to reduce solar heating.

বিমূর্ত

অভিক্ষিপ্ত টারনারি কার্বাইড MAX পর্যায় M_2TlC (M = Ti, Zr, এবং Hf) তাদের ফোনন বিক্ষুরণ এবং অপটিক্যাল বৈশিষ্ট্যগুলির জন্য তদন্ত করা হয়েছে, যার মধ্যে মুলিকেন জনসংখ্যা বিশ্লেষণ, অপটিক্যাল এবং তাত্ত্বিক ভিকার কঠোরতা রয়েছে। আমরা আমাদের গণনার নির্ভুলতা মূল্যায়ন করতে যৌগের কাঠামোগত এবং বৈদ্যুতিক বৈশিষ্ট্য পর্যালোচনা করেছি। পরীক্ষিত MAX পর্যায়গুলি যান্ত্রিকভাবে এবং গতিশীলভাবে স্থিতিশীল, স্থিতিস্থাপক ধ্রুবক, ফোনন বিক্ষুরণ এবং রাজ্যগুলির ফোনন ঘনত্বের পরীক্ষা অনুসারে। Ti-3d, Zr-4d, Hf-5p, 5d, এবং Tl-6p ইলেকট্রনিক অরবিটাল, যা পর্যায়গুলির শারীরিক বৈশিষ্ট্যের উপর যথেষ্ট প্রভাব ফেলে এবং ইলেকট্রনিক পরিবাহনে ব্যাপকভাবে অবদান রাখে, সাব-ব্যান্ড অতিক্রম করার প্রধান কারণ। ইএফ। Ti_2TlC, Zr_2TlC, এবং Hf_2TlC-এর পর্যায়গুলির জন্য, যথাক্রমে, E_F -তে রাজ্যগুলির মোট ঘনত্বের (TDOS) মানগুলি 3.0, 2.55, এবং 2.09 রাজ্য/eV হিসাবে নির্ধারিত হয়। তদন্তাধীন যৌগগুলিতে, সমস্ত বন্ডের মধ্যে Hf-C বন্ধনের সর্বোচ্চ সমযোজীতা রয়েছে। পরীক্ষিত যৌগগুলির কঠোরতা এমনভাবে তুলনা করা যেতে পারে যে Ti_2TlC H_{micro} (24 GPa) এবং H_{macro} (17 GPa) উভয়ের জন্য Hf_2TlC (17 এবং 13 GPa) এবং Zr_2TlC Hf_2TlC (20 এবং 16 GPa) এর চেয়ে কঠিন। যৌগগুলির জন্য Vickers কঠোরতা যথাক্রমে 2.18, 1.61, এবং 2.60 GPa হিসাবে আবিষ্কৃত হয়। রিপোর্ট করা কঠোরতার মানগুলি সুপরিচিত MAX ফেজ ন্যানোলামিনেটের 2 থেকে 8 GPa এর মধ্যে, যেমন Hf_2InC (3.45 GPa) এবং Ta_2InC (4.12 GPa)। Γ-এ অনুদৈর্ঘ্য অপটিক্যাল (LO) এবং ট্রান্সভার্স অপটিক্যাল (TO) উপাদানগুলির মান হল যথাক্রমে 18.66 এবং 19.94 THz (Hf_2TlC), 16.62 এবং 17.18 THz (Zr_2TlC), এবং 19.74 এবং 21.63 THC, THz. সমস্ত তদন্তকৃত যৌগগুলিতে, ফোনন বিক্ষুরণ বক্ররেখাগুলি (সম্পূর্ণ BZ জুড়ে) ফোনন ফ্রিকোয়েন্সি কাল্পনিক (ফ্রিকোয়েন্সি স্কেলে নেতিবাচক) প্রদর্শন করে না, যা পর্যায়গুলির গতিশীল স্থিতিশীলতার পরামর্শ দেয়। 8.76 eV, 9.6 eV এবং 10.7 eV-তে যথাক্রমে Ti_2TlC, Zr_2TlC, এবং Hf_2TlC যৌগগুলির জন্য প্রতিফলিততার মান 92%, 82% এবং 86% পর্যন্ত বেড়ে যায়। এটি একটি চমকপ্রদ পর্যবেক্ষণ যে Ti_2TlC (11.67 eV), Zr_2TlC (12.44 eV), এবং Hf_2TlC (13.8 eV) পর্যায়গুলির জন্য প্রতিফলন সর্বদা 44% এর বেশি। রিফ্লেক্টিভিটির ফলাফল অনুসারে, দৃশ্যমান (1.7 eV-3.3 eV) এবং IR (1.24 eV-1.7 eV) সেক্টরগুলি 12.0 eV পর্যন্ত শক্তির 44%-এর বেশি। অতএব, তদন্তকৃত যৌগগুলি সৌর উত্তাপ কমাতে একটি আচ্ছাদন উপাদান হিসাবে ব্যবহারের জন্য একটি ভাল প্রতিযোগী হতে পারে।

Table of contents

List of Figures

Fig. No. **Figure Caption** **Page No.**

List of Tables

Nomenclature

BFGS	Broyden–Fletcher–Goldfarb–Shanno
BOP	Bond of Population
BZ	Brillouin Zone
CASTEP	CAmbridge Serial Total Energy Package
DF	Density Functional
DFPT	Density Functional Perturbation Theory
DFT	Density Functional Theory
DOS	Density of States
ECP	Effective Core Potential
EVC	Efective Valence Charge
eV	Electron Votls
GGA	Generalized Gradient Approximation
GPa	Giga Pascals
HF	Hartree–Fock
IR	Infrared
KS	Kohn and Sham
LCAO	Linear Combination of Atomic Orbitals
LDA	Local Density Approximation
LDOS	Local Electronic Density of States
LO	Longitudinal Optical
MAP	Mulliken Atomic Population
PBE	Perdew, Burke, and Ernzerhof
PDC	Phonon Dispersion Curves
PDOS	Projected Density of States/Partial Density of States
PP	Pseudopotential
PWPP	Plane Wave Pseudopotential
RPBE	Revised Perdew-Burke-Ernzerhof
SAW	Surface Acoustic Wave
SCF	Self-Consistent Field
BFGS	Broyden–Fletcher–Goldfarb–Shanno
TO	Transverse Optical
UV	Ultraviolet
VEC	Valence Electron Concentration
VRH	Voigt-Reuss-Hill
WDA	Weighted Density Approximation
X_C	Exchange-Correlation

1 Introduction

Researchers are fascinated by the comprehensive study of novel chemicals, which are generally significant and helpful in the field of materials science and technology. Therefore, "MAX Phase" designates a family tree of layered ternary nitrides and carbides with unique properties that combine those of metals and ceramics. This class of materials is very exciting and significant. The value of these materials for use in numerical technology and engineering has expanded as a result of these occurrences. An early transition metal, a group A element, and either C or N are components of the relatively recent family of transition metal layered compounds known as $M_{n+1}AX_n$ (MAX Phase), where n=1, 2, or 3. These ternary compounds preserve highly extraordinary mechanical and chemical properties like excellent thermal and electric conductivity, and machinability thanks to their distinctive structural arrangements. In order to meet the performance requirements of modern materials with applications in technology for the conversion of waste energy, these qualities might be taken into consideration when searching for innovative phases and their composites.

An outline of MAX Phase has been provided in this chapter. The history, characteristics, and applications of the MAX phase as well as a literature review and the goal of the current research activity have all been described.

1.1 Background

1.1.1 MAX phase materials

A phases are a type of ternary layered compounds with the formal stoichiometry $M_{n+1}AX_n$ (n = 1, 2, 3, etc.), where is the transition d metal, is an element from the A-group in groups 12 to 16 of the periodic chart, and X is either carbon or nitrogen. The bulk of MAX phases are 211 phases, while some of them are 312s and some are 413s.

The M, A, and X elements, which can be found in the highlighted portions of the MAX phases materials and are shown in the periodic table of Fig. 1.1 using different colors, are the building blocks of all MAX phases.

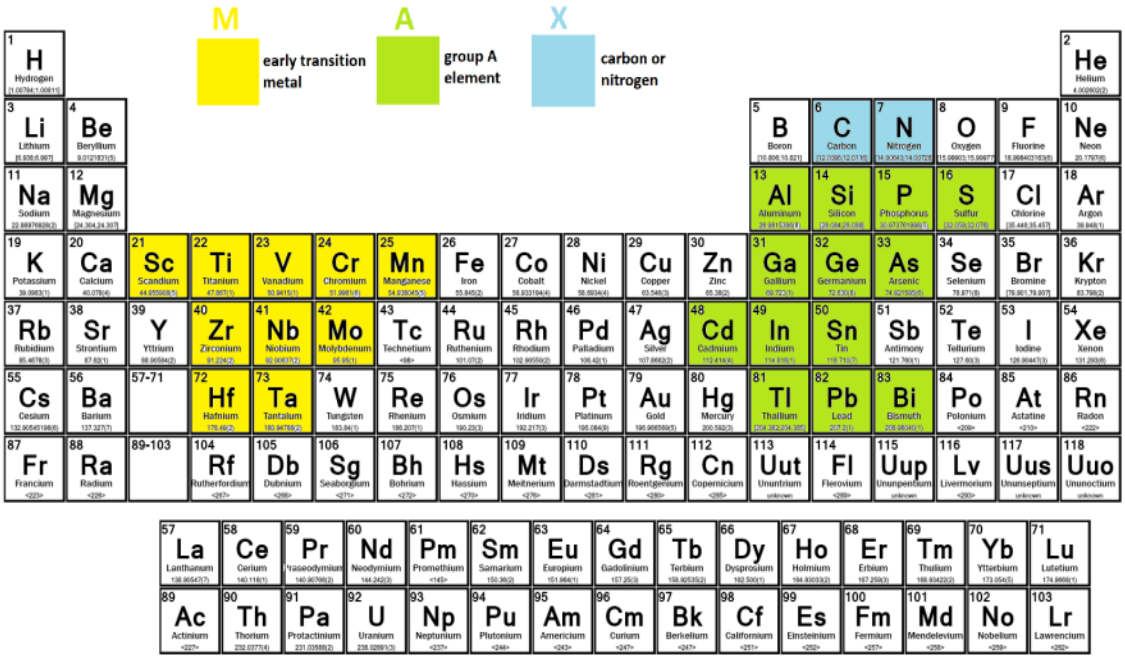

Fig. 1.1 The M, A, and X elements forming all currently known MAX phases.

1.2 Crystal structures of max phase compounds

The MAX phase is characterized by stacked separate atomic layers and a hexagonal crystal lattice with a vertical lattice parameter *c* that is usually 4–8 times longer than the basal plane lattice parameter *a*. Based on the n values in the equation $M_{n+1}AX_n$, these Phases can be divided into several groups. Two M-layers are present between the A layers when n = 1 (Figure 1.2(a)). When n = 2, they are divided into three layers (M_3AX_2 in Fig. 1.2(b)). They are typically referred to as 211, 312 and 413 etc. when n = 3, because they are separated by four layers (M_3AX_2 in Fig. 1.2(c) and so on). With an increase in n value, the lattice gets more complicated, which decreases the thermodynamic stability of the MAX phase relative to rival phases.

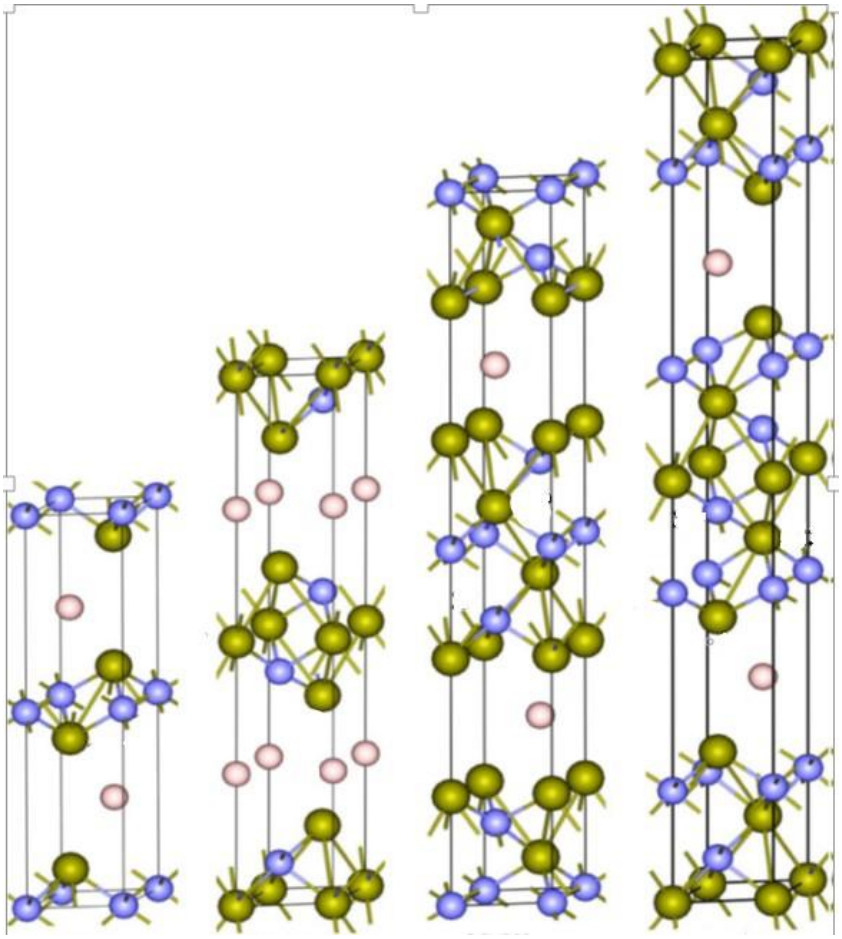

Fig. 1.2 Unit cell of $M_{n+1}AX_n$ MAX Phases for *n*=1 or M_2AX,(a), n=2 for M_3AX_2 (b), n=3 for M_4AX_3 and n=4 for M_5AX_4 phases.

1.3 List of 211 max phase materials

This study focuses on the '211' sub group of the M_2TlC MAX phases where M = Ti, Zr, and Hf. Below is a list of 211 MAX Phase materials to date.

Ti_2CdC, Sc_2InC, Sc_2SnC,Ti_2AlC, Ti_2GaC, Ti_2InC, Ti_2TlC, V_2AlC, V_2GaC, Cr_2GaC, Ti_2AlN, Ti_2GaN, Ti_2InN, V_2GaN, Cr_2GaN, Ti_2GeC, Ti_2SnC, Ti_2PbC, V_2GeC, Cr_2AlC, Cr_2GeC, V_2PC, V_2AsC, Ti_2SC, Zr_2InC, Zr_2TlC, Nb_2AlC, Nb_2GaC, Nb_2InC, Mo_2GaC, Zr_2InN, Zr_2TlN, Zr_2SnC, Zr_2PbC, Nb_2SnC, Nb_2PC, Nb_2AsC, Zr_2SC, Nb_2SC, Hf_2InC, Hf_2TlC, Ta_2AlC, Ta_2GaC, Hf_2SnC, Hf_2PbC, Hf_2SnN, Hf_2SC, Zr_2AlC, Ti_2ZnC, Ti_2ZnN, V_2ZnC, Nb_2CuC, Mn_2GaC, Mo_2AuC, Ti_2AuN

1.4 History of max phase

The history of the MAX phase is divided into two sections. Their first exposure to time began in the early and middle 1960s and ended roughly in the mid-1990s, a time when the majority of the population was ignored. The second period is that of the past 15 or so years, during which time interest in these phases has exploded. The totally densed and pure Ti_3SiC_2 MAX Phase material was created in 1990 by Barsoum and his coworkers, who then characterized it. They allowed it to be exposed so that it would preserve a distinctive combination of some of the best qualities of metals and technical ceramics. One year later, they demonstrated that this compound was only one of more than sixty phases, [1] the majority of which H. Nowotny and colleagues [2] identified and synthesized as powder in the 1960s. When Ti_4AlN_3 was discovered in 1999, researchers recognized they were dealing with a sizable family of solids that all behaved in a similar manner. As a result, there has been a notable progress in our understanding of the characteristics of these phases since 1996. This led the researcher to become preoccupied with the creation, characterization, and use of the MAX Phase family starting in 2006. The unique arrangement of metallic and ceramic characteristics in MAX phases has scientists interested in more research. Without taking into account potential solid solutions, there have previously been identified 48 of the 211 conceivable phases, but more have been theoretically predicted [3], [4–7]. Up to date, there are above 80 MAX phase elements have already been synthesized [5,8–13] and the physical characteristics are also investigated [14–18]. Additionally, very recently the MAX phase materials have been employed as a precursor to create the so-called MXenes, which are atomically thin two-dimensional materials with a variety of appealing physical characteristics [19,20].

1.5 Properties and application

MAX Phases are hence advantageous in materials research and engineering technology due to the rare mix of metals and ceramics features. Due to their special combination of metallic and ceramic properties, the MAX phase nano layered ternary compounds are appropriate for a wide range of technical applications. Similar to metals, they have strong electrical and thermal conductivity, are machinable, have a low hardness, are resistant to thermal shock, and are damage-tolerant. However, these compounds exhibit ceramic properties such high elastic moduli, high melting temperatures, and resistance to oxidation and corrosion [4–7,13,15,17,21]. The metallic properties of the MAX phases are revealed in, for instance, their frequently high electrical and thermal conductivity, high fracture toughness and high machinability, i.e., their ease of cutting, drilling, polishing, etc., allowing them to be used in a variety of technological applications.

They might help create internal combustion engines that are more effective since they can run at higher temperatures than are now feasible. This is because some MAX phases, in contrast to ceramic materials, which are heat resistant but brittle, combine good high temperature characteristics with fracture toughness.

The MAX phase is a good option for optoelectronic devices in the visible and ultraviolet radiation ranges and can be employed as coating materials for electrical contacts, fast spinning devices like turbine blades, and cutting tools to prevent solar heating.

Fig. 1.3: Possible MAX phase applications.

1.6 Context

To recommend a compound for technological applications, a conceptually thorough research of the physical properties of materials is needed. Among these, a material's suitability for practical application can be determined by performing a dynamical stability and mechanical stability examination. Furthermore, it has been important to consider the materials as the foundation of many industrial applications that can be determined readily by the thermodynamic properties [22] because of the compounds' resilience at high temperatures and pressures. For instance, the materials' considerable energy dependence on the refractive index and absorption coefficient as a result of these features is crucial for optoelectronic devices. Furthermore, the reflectivity is a crucial quality to mention when selecting coating materials to reduce solar heating [23]. Investigation of various M_2TlC (M = Ti, Zr, Hf) MAX phase characteristics is therefore anticipated.

As a result, we plan to look at Mulliken analysis, optical properties and Vickers hardness in addition to the material properties of considered compounds.

1.7 Aims and objectives

Due to the MAX Phases are made up of a combination of metallic and ceramic material qualities that make them competitive materials for a variety of applications. Utilizing the special multi-efficient ternary carbides to their full potential in a variety of industrial applications would require a thorough understanding of the association between structure and property as well as the research of physical parameters. Therefore, in order to develop their qualities in solid state physics for technological applications, we must attribute to analysis.

- Optimization of the geometrical structure of the M_2TlC (M= Ti, Zr, Hf) using DFT.
- Study of the structural, elastic, and electronic properties of M_2TlC (M= Ti, Zr, Hf) and discuss in detail.
- Investigation of the optical properties (dielectric function, absorption spectrum, conductivity, energy-loss spectrum, refractive index and reflectivity), mechanical and electronic properties of the compounds.
- The analysis of Mullikin population and Vicker hardness of the ternary carbides M_2TlC (M= Ti, Zr, Hf) will also be studied.

1.8 Significance, scope and definitions

We found that the majority of papers focused on the elastic and structural characteristics of the ternary carbides M_2TlC (M = Ti, Zr, Hf). Vickers hardness, optical and thermodynamic properties, as well as Mulliken populations, have not been taken into consideration.

Numerous studies of the M_2AX phases have been conducted, both theoretically and experimentally, but only a handful have been completed. There aren't many investigations on the compounds' M_2TlC (M = Ti, Zr, Hf) MAX phases, despite their technological importance. Ta_2InC (TIC) has not yet been synthesized or thoroughly researched, unlike the phases Zr_2InC (ZIC) and Hf_2InC (HIC), which have both already been created.

The physical qualities of a compound must be thoroughly investigated theoretically in order to recommend it, particularly for technological applications. The study of a material's dynamical stability is crucial for practical application under high pressure and temperature circumstances. Additionally, the thermodynamic properties offer significant additional data about how materials behave under high pressures and temperatures, which is thought to be the foundation of many industrial applications [24]. The electronic characteristics of materials, which display the electronic reaction of the materials exposed to radiation, are intimately related to the optical properties. The knowledge of a material's refractive index and absorption coefficient is required to choose a material for optoelectronic devices [25]. Additionally, it is possible to forecast which materials will be effective as coating materials to lower solar heating by studying the reflectivity of MAX phases [26]. Therefore, both from a research and an application standpoint, it is desirable to explore these physical characteristics of M_2TlC (M = Ti, Zr, Hf) MAX phases.

We feel compelled to thoroughly explore M_2TlC (M = Ti, Zr, Hf) MAX phases' dynamical stability, thermodynamics, and optical properties for the first time. In addition, the structural, elastic, and electrical properties are discussed along with Mulliken analysis, optical properties and Vickers hardness.

1.9 Thesis outline

The thesis is organized as follows:

- Chapter 1 covers the introduction, definition, history, and list of MAX Phase materials, as well as the motivation for and goals of the current study and a brief discussion of related past work.
- A brief summary of the structural characteristics of MAX phase materials is provided in Chapter 2.
- Chapter 3 provides a description of the theoretical approach used in this study.
- The computation of various MAX phase materials' properties is covered in Chapter 4.
- The findings of the study's numerous investigations are reported in chapter 5 along with a brief discussion.
- Chapter 6 of the current work contains a conclusion.

2 Literature review

Researchers' interest in the MAX Phases has grown as a result of their peculiar characteristics related to metals and ceramics. On the MAX Phase, numerous research projects have been carried out. Here are a few review articles that are closely relevant to the current investigations:

A. Bouhemadou et al. reported “first-principles calculations utilizing the pseudo-potential plane-waves approach were used by to examine the structural and elastic properties of Sc_2AC, where A = Al, Ga, In, and Tl. In order to calculate the exchange-correlation approximation energy, the calculations were done using the LDA. They measured the impact of high pressures up to 20 GPa on the predicted internal parameters and lattice constants. They also calculated the Young's moduli, Poisson's ratio, bulk and shear moduli, and Young's moduli for perfect polycrystalline Sc_2AC aggregates. [27]

“The elastic constants for 240 elemental compositions of the huge M_2AX (M=Sc, Ti, Zr, Hf, V, Nb, Ta, Cr, Mo and W), A=Al, Ga, In, Tl, Si, Ge, Sn, Pb, P, S and As), X=C or N] phase family of nanolaminate ceramics have been calculated” by M. F. Cover et al. “They have provided and debated in-depth studies of the data's correlations. These show how different elastic and structural properties connect to one another within the MAX phase family and how the choice of constituents affects them. In particular, the correlations show how the A element governs the process and interacts with the M element to determine the material's compressibility and shear ability along the c axis. The in-plane constants C_{11} and C_{12} exhibit the X element's biggest influence, which is relatively negligible. These results provide methods for modifying the elastic behavior of the M_2AX phases through the careful selection of M, A, and X elements.” [28]

"The Sc_2AC computations using A=Al, Ga, In, and Tl were performed" by D. Music et al. "The hybridization of C 2p and Sc 3d and A p and Sc 3d states has been demonstrated, but the antibonding states start to emerge at about 0.4 eV, decreasing the total bonding. The size of the A element has a little impact on chemical bonding. These phases could be categorized as weakly coupled MAX phases based on the fact that the constituent ScC's bulk modulus is not conserved." [29]

S. Gupta et al. described "the ternary carbide Zr_2InC's synthesis and oxidation behavior. Utilizing thermogravimetric oxidation kinetics in air at 400–700 °C, they were studied. The reaction resulted in In_2O_3, which probably contained some dissolved transition metal ions, and the transition metal oxides. They were either amorphous or nanocrystalline in nature. The oxidation occurred as a result of oxygen's inward migration." [30]

B. Manoun et al. investigated "using a synchrotron radiation source and a diamond-anvil cell, the lattice parameters of a polycrystalline Zr_2InC sample have been determined in relation to pressure. Up to a pressure of 52 GPa, no phase transitions were noticed. They discovered that Zr_2InC was more compressible along the c-axis than the a-axis. With a pressure derivative of 4250 and a bulk modulus of 1275 GPa, the result is in very good agreement with ab initio estimates (130.9 GPa). The ab initio calculations' results for the parameters a (3.367) and c (15.100) are also somewhat bigger than the observed values of 3.35 and 14.91." [31]

"The characterisation of Hf_2InC ($Hf_{1.96}InC_{1.26}$) samples made by reactive hot isostatic pressing of the elemental powders was reported" by M. W. Barsoum et al. "for Hf_2InC, they discovered the nm values of 0.331 and 1.472 for the *a* and *c* lattice parameters. As a function of temperature, the heat capacities, thermal expansion

coefficients, and thermal and electrical conductivities were also measured. This ternary exhibit good electrical conductivity, and its resistance rises linearly as temperature rises. The thermal expansion coefficient for Hf_2InC is 7.6310 K in the temperature range of 300 to 1273 K" [32]

According to Y. Medkour et al., "they investigated the structural and electronic properties of a subset of M_2InC compounds that belong to the so-called MAX phases, with M = Ti, Zr, and Hf, using a pseudopotential plane waves technique based on density functional theory inside the generalized gradient approximation. They observed the effect of high pressures, up to 50 GPa, on the lattice constants and found that the contractions along the c-axis were larger than those along the *a* axis. The examination of the band structure and density of states as well as the derived elastic constants, demonstrate that these compounds are electrical conductors. The hybridization of the M-atom d states with the C-atom p states ensures a strong directed link between the M and C atoms. Additionally, they looked into how bond lengths were affected by hydrostatic pressure, finding that in the order of Ti_2InC, Zr_2InC, and Hf_2InC, M-C and M-In bonds became stronger while M-In bonds shorten."[27]

"Ti_2InC, Zr_2InC, and Hf_2InC's MAX phases' lattice constants, bulk moduli, and total- and partial-density of states have all been calculated using ab initio methods" stated by X. He et al. "Lattice constants have variations from experimental values that are less than 1.6%. According to calculations, the bulk moduli are 128 GPa, 113 GPa, and 136 GPa, respectively. Among the MAX phases investigated to date, the Zr_2InC has the lowest bulk modulus, which is due to the weaker covalent connection between Zr-d and C-s, C-p states" [33]

A. Bouhemadou et al. investigated “the structural and elastic properties of M_2InC, where M = Sc, Ti, V, Zr, Nb, Hf, and Ta by using ab initio calculations.” “The lattice parameters were found to depend quadratically on the applied pressure. The static finite strain method is used to calculate the elastic constants. For ideal polycrystalline M_2InC aggregates, they also deduced the bulk and shear moduli, Young's moduli, and Poisson's ratio. The experimental verification of this first quantitative theoretical prediction of the elastic characteristics of the compounds Sc_2InC, Ti_2InC, V_2InC, Zr_2InC, Nb_2InC, Hf_2InC, and Ta_2InC is still pending” [22].

J. A. Warner et al. used “ab initio calculations to determine the lattice constants, bulk moduli, and local and total densities of states of the MAX phases Ti_2TlC, Zr_2TlC, and Hf_2TlC, belongs to the hexagonal P63/mmc space group.” “In their research, scientists discovered that all three materials conduct electricity, with the density of states (DOS) at Fermi energy dropping as the transition metal's atomic number increases. They demonstrated that these substances have the lowest anticipated bulk moduli of 125, 120, and 131 GPa, respectively. These are the lowest bulk moduli among the MAX phases now under experimental or theoretical study. They discovered that all three materials are conducting based on the electronic density of states. The weak metal M (M= Ti, Zr, or Hf) bonding with the A element thallium is responsible for these low values of their bulk moduli” [23].

H. Bolvardi et al. examined “the electrical structure and mechanical properties of the phases X_2BC with X = Ti, V, Zr, Nb, Mo, Hf, Ta, and W (Mo_2BC-prototype) using ab initio calculations. As the valence electron concentration (VEC) per atom increased by substituting the transition metal X, they discovered that the six extraordinarily strong bonds between the transition metal and the carbon changed to

lower energies relative to the Fermi level. As a result, the bulk modulus increased to values as high as 350 GPa, or 93% of the value recorded for c-BN. Systems with higher VEC are likely ductile, according to both the bigger positive Cauchy pressure and the higher value of the bulk to shear modulus ratio (B=G). Smaller unit cells have higher orbital overlap, which results in more delocalized interatomic interactions and more ductile behavior. The computed phase stabilities show an increasing trend as the VEC is shrunk. Because of their relatively unusual combination of high stiffness and mild ductility, the X_2BC compounds with X= Ta, Mo, and W are excellent choices for safeguarding cutting and shaping tools."[34]

3 Materials and methodology

3.1 Introduction

Compared to other methods, ab initio calculations can produce high-quality quantitative predictions for a variety of systems. In order to investigate structural and electronic properties, calculations were made using the ab initio plane wave pseudo potential (PW-PP) method within the framework of density functional theory (DFT) [35] implemented in CASTEP code [36]. The present chapter goes into great detail about these exacting mathematical processes used in ab initio approaches.

3.2 Ab initio method

The phrase "ab initio" means "from the beginning" and is derived from the Latin words "ab" (from) and "initio," an ablative of initium (beginning).

The most common categories of ab initio techniques are: Hartree-Fock (HF) method [37–39] and DFT [35,40]. We are concentrated only for DFT in this study.

3.2.1 Density functional theory (DFT)

The two theorems that Hohenberg and Kohn proved in 1964 [41] and the computational scheme that Kohn and Sham (KS) proposed the following year [42] form the foundation of density functional (DF) techniques. They demonstrated how the electron density affects the overall energy. This means that the essential concept in density functional theory. Electron density are must be understood instead of the challenging many electron wave function.

Theorem 1 (Uniqueness): The exact ground state electron density $\rho_o(\boldsymbol{r})$ is a unique functional of the ground state expectation value of any observable. This indicates that it is possible to compute all of the system's properties in the ground state if the electron density and functional are known. In particular, the ground state energy $E_o[\rho_o(\boldsymbol{r})$ can be calculated.

Theorem 2: The principle of variation The total energy functional E [ρ]. is minimized by (r). Thus, with a specific external potential generated by a set of nuclear charges, the second theorem offers a variational condition for calculating ρo(r) and Eo [ρ] jointly.

e.g. $V(\boldsymbol{r}) = -\sum_{i,j=1}^{N_{el}N_{at}} \frac{Z_j}{|r_i - \boldsymbol{R}_j|}$

E_0 is found by minimizing an expression of the form [20]:

$$E[\rho(\boldsymbol{r})] = \int \rho(\boldsymbol{r}) V(\boldsymbol{r}) d\boldsymbol{r} + \frac{1}{2}\int \frac{[\rho(\boldsymbol{r})\rho(\boldsymbol{r}']}{|\boldsymbol{r} - \boldsymbol{r}'|} d\boldsymbol{r} d\boldsymbol{r},$$

$$+\int \rho(\boldsymbol{r})\, g(\mathbf{r};[\rho])\, d\mathbf{r} + \sum_{i,j=1}^{N_{at}N_{at}} \frac{Z_i Z_j}{|\boldsymbol{R}_i - \boldsymbol{R}_j|}$$

$$= E_{ext} + E_j + E_{kxc} + E_{Rep} N_{uc} \tag{3.1}$$

with regard to an arbitrary function, r, which stands for the density of n electrons. The self-consistent field (SCF) method is used in the Kohn and Sham (KS) method to determine the ground state energy as follows:

1. For the one-electron effective Hamiltonian, the n/2 lowest eigen values and related Eigen functions (orbitals) are discovered:
2. $$\hat{h_{eff}}\psi_i(\boldsymbol{r}) \equiv \left[-\frac{1}{2}\nabla^2 + Ve_{ff}(\boldsymbol{r})\right]\psi(\boldsymbol{r}) = \varepsilon_i \psi_i(\boldsymbol{r}) \tag{3.2}$$

1. The calculation of density, $\rho(\boldsymbol{r})$:

$$\rho(\boldsymbol{r}) = 2\sum_{i}|\Psi_i(\boldsymbol{r})^2|$$

2. The re-calculation, V_{eff} as a function of the density, $\rho(\boldsymbol{r})$:

$$V_{eff}(\boldsymbol{r}) \;\; V(\boldsymbol{r}) + \int \frac{\rho(\boldsymbol{r}'}{|\boldsymbol{r}-\boldsymbol{r}'|} d\boldsymbol{r}' + \mu_{xc}(\boldsymbol{r};[\rho]) \tag{3.3}$$

Where $\mu_{xc}(\boldsymbol{r};[\rho])$ is the exchange-correlation potential.

3. If self-consistency is not reached, go to step 1.

4. At self-consistency, $\rho(\boldsymbol{r}) = \rho_0(\boldsymbol{r})$ (GS density) and the ground state energy can be calculated by the following equation,

$$E_0 = E_{kps} + \int \rho_0(\boldsymbol{r})V(\boldsymbol{r})d\boldsymbol{r} + \frac{1}{2}\int \frac{\rho_0(\boldsymbol{r})\rho_0(\boldsymbol{r}')}{|\boldsymbol{r}-\boldsymbol{r}'|} d\boldsymbol{r}\, d\boldsymbol{r}$$

$$+E_{xc} + E_{Rep}N_{uc} \tag{3.4}$$

where the pseudo-kinetic energy, E_{kps} is defined by,

$$E_{kps} \;=\; \sum_i \int \psi_i\,(\boldsymbol{r})^* \left(-\frac{1}{2}\nabla^2\right)\psi_i(\boldsymbol{r})d\boldsymbol{r} \tag{3.5}$$

and the exchange-correlation energy, E_{xc} is expressed as,

$$= E_{ext} + E_j + E_{kxc} + E_{Rep}N_{uc} \tag{3.6}$$

The Effective Core Potential (ECP) can be calculated by the following equation [43]:

$$E^{DFT} = \int \varepsilon^{DFT}(\boldsymbol{r})\mathrm{d}\boldsymbol{r} \tag{3.7}$$

is a precise integration that must be used to determine the electron-electron interaction's contribution to energy in the periodic density functional theory (DFT) within the linear combination of atomic orbitals (DFT-LCAO) approach [44].

3.2.1.1 Local density approximation (LDA)

Typically, an LDA for the exchange-correlation energy in a spin-unpolarized system is expressed as,

$$E_{xc}^{LDA}[\rho] = \int \rho(\boldsymbol{r})\epsilon_{xc}(\rho)d\boldsymbol{r} \tag{3.8}$$

Where ρ is the electronic density and $\in_{xc}$, the exchange-correlation energy density, is a function of the density alone. The exchange-correlation energy is decomposed in to exchange and correlation terms linearly,

$$E_{xc} = E_x + E_c \tag{3.9}$$

so that separate expressions for E_x and E_c are sought.

3.2.1.2 Generalized gradient approximation (GGA)

The Generalized Gradient Approximation (GGA) has been used in this study's DFT calculations. Local density approximation is less effective than the generalized gradient approximation (GGA). The GGA has shown to outperform LDA in systems where the charge density is slowly changing. It also applies to the inhomogeneous electron gas system. The exchange-correlation energy Exc is a function of the spin density and their gradients [44] and can thus produce the more relevant results.

$$[\rho\alpha, \rho\beta] = \int[\rho\alpha(\boldsymbol{r}), \rho\beta(\boldsymbol{r}), \nabla\rho\alpha(\boldsymbol{r}), \nabla\rho\beta(\boldsymbol{r})]d\boldsymbol{r} \tag{3.10}$$

The introduction of GGA is intended to greatly raise the caliber of LDA results.

3.3 Pseudopotentioals

In order to have the modified effective potential term appear in the Schrödinger equation instead of the Columbic potential term for core electrons that is typically

present in the Schrödinger equation, the pseudopotential is an attempt to replace the complex effects of the motion of the core (i.e., non-valence) electrons of an atom and its nucleus with an effective potential, or pseudopotential. The pseudopotential approximation was created in the 1930s by Hans Hellmann.

There are two types of Pseudo potentials:

1. Norm-conserving pseudopotential
2. Ultrasoft pseudopotential

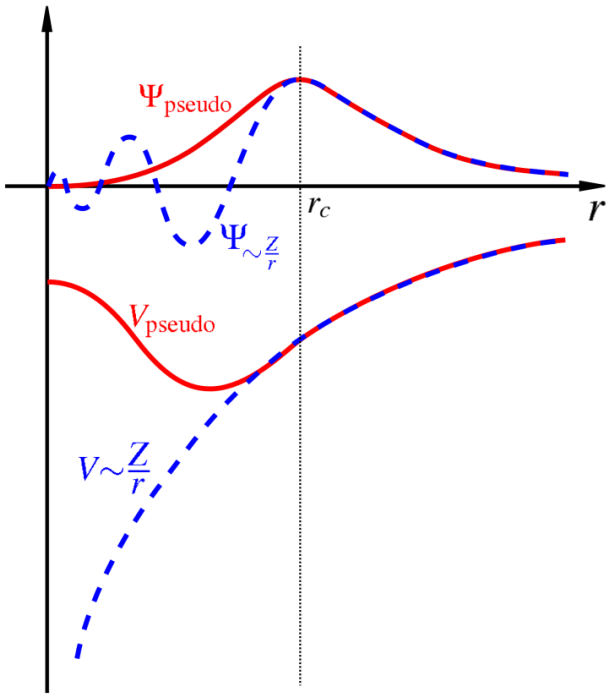

Fig. 3.1: A schematic illustration of all-electrons (blue lines) and pseudo- (red lines) potentials and their corresponding wavefunctions. The radius at which all-electrons and pseudopotentials values match is r_c (26).

3.4 CASTEP code

The density functional theory (DFT) [35], as embodied in the CASTEP program code [36], was used to optimize the M_2TlC (M = Ti, Zr, Hf) unit cell and its physical attributes. The functional is used to represent the exchange-correlation potential using the Perdew-Burke-Ernzerh (PBE) of Generalized Gradient Approximation (GGA) [45]. The interaction between electron-ions potentials are preserved within Vanderbilt-type ultrasoft formulation [46] for M (Ti, Zr, Hf), Tl, and C atoms. The convergence is confirmed by changing the plane's energy cut-off to 400 eV and using the Monkhorst-Pack mesh for the 7×7×2 k-point samplings [47]. The tolerance is used for the geometry optimization for self-consistent field 5.0×10^{-7} eV/atom, maximum force on the atom 0.01 eV/Å, highest movement of atom 5×10^{-4} Å, and maximum stress 0.02 GPa. The optimization of atomic configuration is employed using BFGS [48].

Calculation of forces, stresses, elastic constants, and total energy are only a few examples of the physical properties of materials that may be calculated using CASTEP. Subject to the typical band gap considerations of DFT, electronic structure also includes optical properties (such as reflectivity, absorption, refractive index, and dielectric function), electronic charge densities, orbitals, electrostatic potentials, band structure, total and partial electronic density of states, Mulliken population analysis, and band structure. The flow chart for the solving Kohn-Shams equation as follows

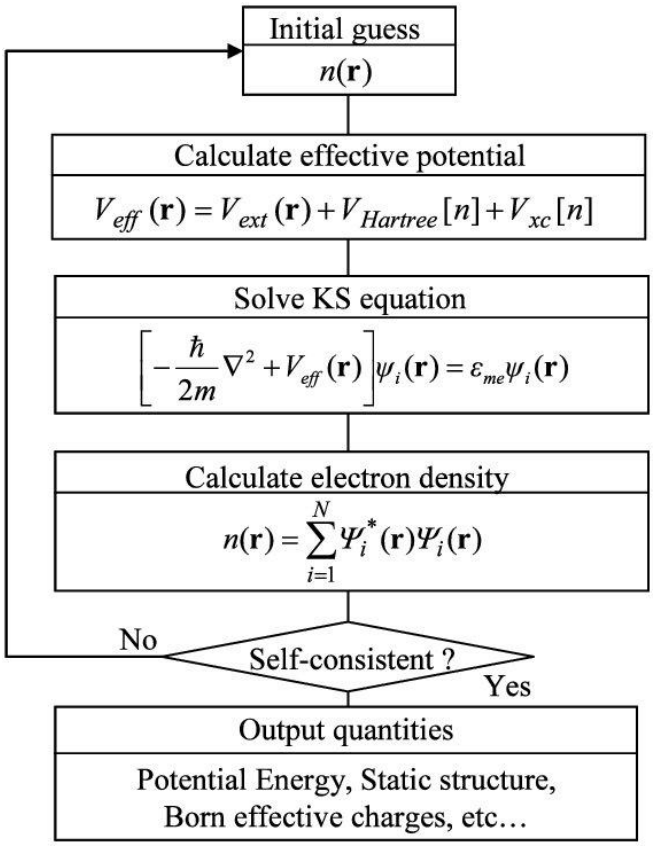

We have examined the system's ground state electron density. With the aid of additional potentials, this density is utilized to compute the effective potential (V_{eff}), also known as the Kohn-Sham potential. In order to compute the Kohn-Shams equation for non-interacting particles, the V_{eff} is added to the Hamiltonian. Our program is finished if the newly computed electron density satisfies our requirement; if not, it will continue to calculate until convergence is reached. Whenever we achieve final energy where the system is converged, we would be able to calculate other properties of the system.

4 Results and discussion

4.1 Introduction

The computational findings of the inquiry into the physical characteristics of the MAX phase ternary carbide M_2TlC (M = Ti, Zr, Hf) are provided in this chapter. We have performed first principles pseudo potential calculations for the first time to investigate the phonon dispersion, thermodynamic, and optical properties of MAX phases M_2TlC (M = Ti, Zr, Hf), including Mullikan population analysis, and theoretical Vickers hardness. Although M_2TlC's lattice parameters, bulk modulus and local electronic density of states (LDOS) have already been examined [22,23], we evaluated these properties together with the compound's structural, elastic, and electronic characteristics to evaluate the accuracy of our calculations. Additionally, we looked into the elastic constants, total and partial densities of states, and bulk modulus. With the aid of a well-established formalism, calculations and discussions of the technically significant optical constants dielectric function, refractive index, photoconductivity, absorption coefficients, loss function, and reflectivity are made.

4.2 Geometry optimization

By using the cut-off energy as input in the CASTEP code with zero pressure, the values of unit cell volume and enthalpy of the ternary carbides M_2TlC (M = Ti, Zr, Hf) compounds have been determined and are shown in Figure 4.1. To choose the best cut-off energy for the compounds, we optimize the shape to reduce the total energy of the unit cell. As the cut-off energy increases, the cell volume and enthalpy steadily decrease as illustrated in Table 4.1. The convergence is confirmed by changing the plane's energy cutoff to 400 eV and using the Monkhorst-Pack mesh for the 7×7×2 k-point samplings [47]. The tolerance is used for the geometry optimization for self-consistent field

5.0×10^{-7} eV/atom, maximum force on the atom 0.01 eV/Å, highest movement of atom 5 $\times$ 10^{-4} Å, and maximum stress 0.02 GPa. The optimization of atomic configuration is employed using Broyden–Fletcher–Goldfarb–Shanno (BFGS) [48].

4.2.1 Stability of the structure

The unit cell of M_2TlC (M =Ti/Zr/Hf) is shown in Figure 4.1. It crystallizes in the P63/mmc (194) space group, which is a part of the hexagonal structure. M (Ti/Zr/Hf), A (Tl), and C's atomic positions in the unit cell are (1/3, 2/3, z_M), (1/3, 2/3, 3/4), and (0, 0, 0), respectively [22,23]. The parameters of relaxed structure at optimum condition are shown in Table 4.1. The obtained results show a very low deviation (within less than 2%) from reported values that proves our calculation are well consistence and good agreement with previously published outcomes [22,23,48].

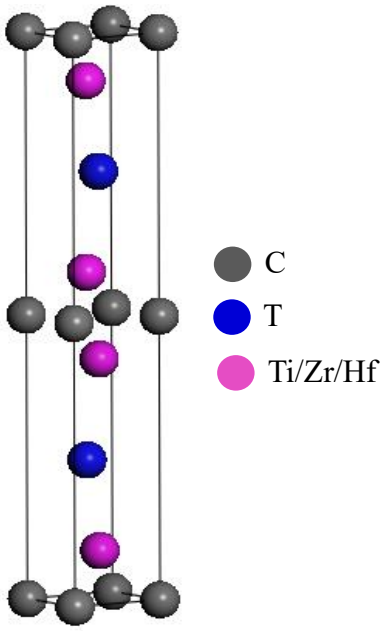

Fig. 4.1: The cell structure of M_2TlC (Ti_2TlC, Zr_2TlC and Hf_2TlC).

Table 4.1. Calculated lattice parameters *a*(Å), cell volume *V* (Å^3), internal parameter z_M of the M_2TlC (Ti_2TlC, Zr_2TlC and Hf_2TlC) compounds.

Phases	*a*	% of deviation	*c*	% of deviation	*c/a*	% of deviation	z_M	V	Ref.
Ti_2TlC	3.18	1.0	14.19	1.5	4.46	0.54	0.079	124.19	This work (GGA)
	3.17	0.6	14.20	1.6	4.48	0.93	0.079		GGA [22,23]
	3.15		13.98		4.44				Expt. [49]
Zr_2TlC	3.39	0.9	15.16	1.1	4.47	0.24	0.0809	150.76	This work (GGA)
	3.37	0.3	15.07	0.5	4.47	0.24	0.0809		GGA [22,23]
	3.36		14.99		4.46				Expt.[49]
Hf_2TlC	3.38	1.8	14.86	0.5	4.40	1.24	0.0825	147.25	This work (GGA)
	3.37	1.5	14.85	0.5	4.41	1.02	0.0825		GGA [22,23]
	3.32		14.78		4.45				Expt. [49]

Before studying different parameters, stability check of the structure is very much important either experimentally or theoretically. We used two strategies: phonon dispersion for dynamical stability and stiffness constants for mechanical stability (C_{ij}). Ti_2TlC, Zr_2TlC, and Hf_2TlC combinations' phonon dispersion curves (PDC) are calculated using DFPT along the crystal's Brillouin zone's (BZ) high symmetry orientation (Density Functional Perturbation Theory) and illustrate them in Fig.4.2 (a-f). The PDC shows frequencies over the range of wave vector (*k*) are in positive values, i.e., no negative frequency exhibits over *k* that indicates all studied compounds are dynamically stable. The PDC curves show distinct transverse optical (TO) and longitudinal optical (LO) components, which are accountable for the solid's optical response. The values of TO and LO at are 19.74, 21.63 THz (Ti_2TlC), 16.62, 17.18 THz (Zr_2TlC) and 18.66, 19.94 THz (Hf_2TlC), respectively. The phonon DOS of Ti_2TlC, Zr_2TlC and Hf_2TlC phases are placed next to one another for clear thoughtful in Figs.4.2 (b, d, f), respectively, where flat band produces noticeable peak and weak arises from non-flat.

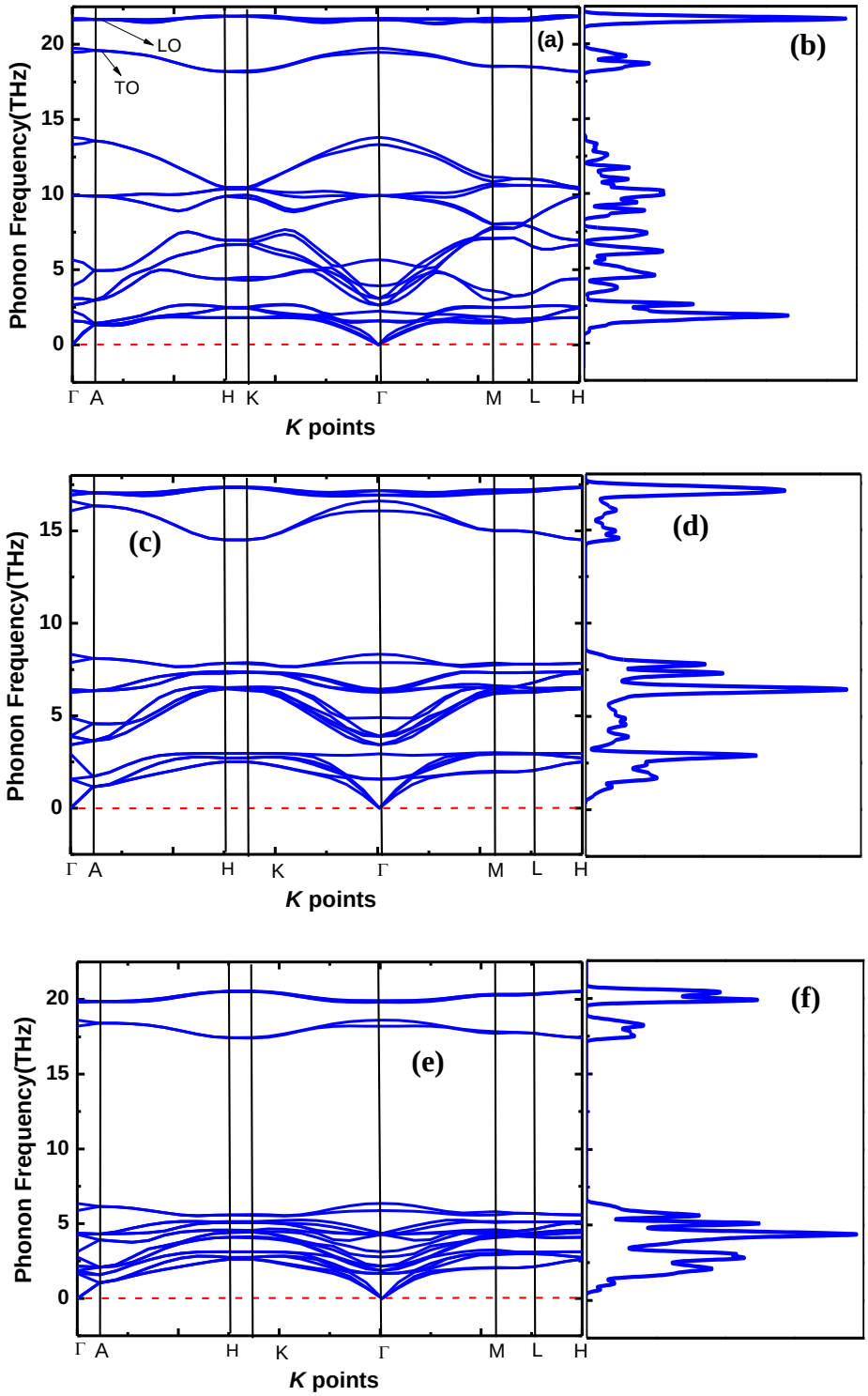

Fig. 4.2: The PDC and PHDOS (phonon density of state) of Ti_2TlC (a,b), Zr_2TlC (c,d) and Hf_2TlC (e,f) compounds. Red dashed line represents zero phonon frequency.

4.2.2 Thermodynamic stability

We have calculated the formation energy to ensure the thermodynamic stability of the studied phases using the following equation[50]:

$$E_{for}^{M_2TlC} = \frac{E_{total}^{M_2TlC} - (xE_{solid}^{M} + yE_{solid}^{Tl} + zE_{solid}^{C})}{x + y + z} \; ; \; M = \text{Ti, Zr, Hf}$$

Here $E_{total}^{M_2TlC}$ is the total energy of the compound after optimization of the unit cell. E_{solid}^{M},E_{solid}^{Tl}, E_{solid}^{C} are the energy of the single phase M, Tl, C respectively. The *x*, y, z is the number of atoms in the unit cell for M, Tl, and C respectively, i.e., *x*=4, y=2, and z=2. The minimum formation energy values for Ti_2TlC, Zr_2TlC, and Hf_2TlC are found to be -0.5881083 eV/atom, -0.682486 eV/atom, and -0.6163068 eV/atom, respectively. The negative sign of obtained values indicates the M_2TlC MAX phases can be experimentally synthesized.

4.3 Mechanical properties and hardness

Cracks are anticipated to be avoided whenever the materials are used for practical purposes. The reaction or deformation of a material to the application of a load or force is revealed by the material's mechanical characteristics. Stiffness, strength, elastic moduli, micro and macro hardness, ductility, and toughness are important factors that define a material's mechanical qualities. The mechanical properties characterizing parameters can be used to understand the fundamental information that is necessary to choose the materials for engineering applications, including elastic moduli, stability, stiffness, brittleness, and ductility of a material. Estimated and provided in Table 4.2.are five separate elastic constants C_{ij} and polycrystalline elastic moduli, as well as any available recorded evidence [23,48] that shows the estimated elastic constants are not in decent agree with past findings. The determined C_{ij}'s meet the mechanical stability requirements for the hexagonal system[51]: $C_{11} > 0$, $C_{11} > C_{12}$, $C_{44} > 0$, $(C_{11} + C_{12})\, C_{33}$-

$2C_{13} > 0$. This supports the MAX phases M_2TlC's mechanical stability (Ti_2TlC, Zr_2TlC and Hf_2TlC).

Table 4.2. The calculated elastic constants, C_{ij} (GPa), various moduli [bulk B (GPa), shear, G (GPa), shear anisotropy constant, A, Young's, Y (GPa)], Pugh ratio, G/B, and Poisson ratio, ν of MAX phases Ti_2TlC, Zr_2TlC and Hf_2TlC compounds.

Phases	**C_{11}**	**C_{12}**	**C_{13}**	**C_{33}**	**C_{44}**	***A***	**B**	**G**	**Y=9 B_HG_H /(3B_H +G_H)**	**G/B**	**MI**	***H_{micro}***	***H_{macro}***	**ν=(3B_H−Y_H)/ 6B_H**	**Ref**
Ti_2TlC	274	73	51	241	82	0.82	126	93	248	0.74	1.54	24	17	0.163	This
	275	73	46	223	72	0.71	123	86	210	0.70	1.71	17	15	0.210	[23] GGA
Zr_2TlC	239	69	56	204	69	0.81	115	78	211	0.68	1.67	17	13	0.207	This
	255	60	52	270	70	0.72	117	78	195	0.67	1.67	15	13	0.219	[23] GGA
Hf_2TlC	278	68	64	245	81	0.77	132	93	252	0.70	1.63	20	16	0.208	This
	278	69	62	230	71	0.68	129	86	214	0.67	1.82	16	14	0.225	[23] GGA

It can be seen that C_{11} indicates how much resistance there is for distortion toward the a-axis, whereas C_{33} indicates toward the c-axis. The obtained C_{11} of Ti_2TlC and Hf_2TlC is found to be higher than that of Zr_2TlC, contrary to expectations, as a result of their greater stiffness, resistance to distortion along the a-axis, and bonding strength. Compounds Ti_2TlC and Hf_2TlC display significantly higher C_{44} values than Zr_2TlC, which findings in optimum shear modulus (G), as tabulated in Table 4.2. The C_{44} values are connected to shear deformation and damage tolerant response. The C_{ij} (single-crystal elastic constants) and its corresponding compliance tensors S_{ij} ($S_{ij} = C_{ij}^{-1}$) are utilized to assess the elastic moduli *B*, *G*, *Y*, and *v* by the equation: $Y = \frac{9B_HG_H}{(3B_H+G_H)}$ and $\upsilon = \frac{(3B_H-Y_H)}{6B_H}$ [52]. The calculated findings are listed in Table 4.2. and elastic moduli (*B, G, Y*) have been represented by Voigt-Reuss-Hill (VRH) [53,54] equations as: $B_V = \frac{[2(C_{11}+C_{12})+C_{33}+4C_{13}]}{9}$ and $G_V = \frac{[C_{11}+C_{12}+2C_{33}-4C_{13}+12C_{44}+12C_{66}]}{30}$, $B_R = \frac{(C_{11}+C_{12})C_{33}-2C_{13}^2}{C_{11}+C_{12}+2C_{33}-4C_{13}}$

and $G_R = \frac{\left(\frac{5}{2}\right)[C^2 C_{44} C_{66}]}{[3B_V C_{44} C_{66} + C^2(C_{44}+C_{66})]}$, $C^2 = (C_{11}+C_{12})C_{33} - 2C_{13}^2, C_{66} = \frac{C_{11}-C_{12}}{2}$, Hill's value is defined by the mean of higher limit of Voigt and lower limit of Reuss as $B_H = \frac{B_R + B_V}{2}$ and $G_H = \frac{G_R + G_V}{2}$. The calculated Paugh ratios G/B for brittle materials G/B > 0.57 while its ratio in ductile materials $v < 0.57$. Poisson's ratios for Zr_2TlC, Ti_2TlC and Hf_2TlC compounds were 0.207, 0.163 and 0.208, respectively, which are smaller than the value of Frantsevich's criteria (0.26) [55] , showing that the examined compounds are brittle.

An additional statistic taken into account while studying anisotropy is the universal anisotropic index (A^U). Utilizing the results from the Voigt and Reuss models of B and G, the following formula is utilized to obtain the A^U.[56]:

$$A^U = 5\frac{G_V}{G_R} + \frac{B_V}{B_R} - 6 \geq 0.$$

The values of A^U are found to be 0.073, 0.367 and 0.077 for the phases Ti_2TlC, Zr_2TlC and Hf_2TlC, respectively. If A^U do not equal zero, the materials will lose their isotropic properties and become anisotropic. Therefore, it is determined that the compounds under study are anisotropic based on the non-zero values of the aforementioned parameters.

Table 4.3. Calculated shear anisotropic A_{100}, A_{010} and A_{001} of Ti_2TlC, Zr_2TlC and Hf_2TlC compounds.

Phases	A_{100}	A_{010}	A_{001}	A^U
Ti_2TlC	0.78	0.82	0.64	0.073
Zr_2TlC	0.90	0.71	0.64	0.367
Hf_2TlC	0.70	0.81	0.56	0.077

We have estimated shear anisotropic factors as shown in Table 4.3 that are expressed for hexagonal solids: $A_1 = \frac{1/6(C_{11}+C_{12}+2C_{33}-4C_{13})}{C_{44}}$, $A_2 = \frac{2C_{44}}{C_{11}-C_{12}}$, $A_3 = A_1.A_2 = \frac{1/3(C_{11}+C_{12}+2C_{33}-4C_{13})}{C_{11}-C_{12}}$ for the {100}, {010} and {001} planes, respectively [55]. If $A_{\{100\}}$, $A_{\{010\}}$ and $A_{\{001\}}$ show unit value (one) that indicates solid is isotropic in nature otherwise exhibits anisotropic and deviation from one provides the level of anisotropy. The calculated factors indicate the studied compounds retain anisotropy property.

Along with 2D images, a 3D contour map can be used to confirm the compounds' anisotropy. It is easier to comprehend the anisotropic behavior by using contour plots (3D) and their two-dimensional (2D) counterparts. Young's modulus, compressibility, shear modulus, and Poisson's ratio are among the variables listed in Table 4.4. that can be utilized to evaluate the degree of anisotropy. These are computed using the ELATE open-source software and displayed in 2D and 3D contour plots, respectively [57].

Only plots for the Ti_2TlC phase are shown in Fig. 4.3 since the plots for the examined compounds are almost identical. The values of Y, G, and are strongly anisotropic and deviate from circles in 2D perspective and spherical shapes in 3D, respectively. This is consistent with the estimated values of *A* in Table 4.3. and shows the phases to be strongly anisotropic. In the *yz* and *xz* planes, Y's value is anisotropic, whereas it is isotropic in the *xy* plane. The anisotropy factor (*A*) is calculated by dividing the higher and lower values of Y, G, and [45] by the degree of anisotropy (Table 4.3). Compared to Zr_2TlC and Hf_2TlC compounds, the Ti_2TlC phase is more anisotropic.

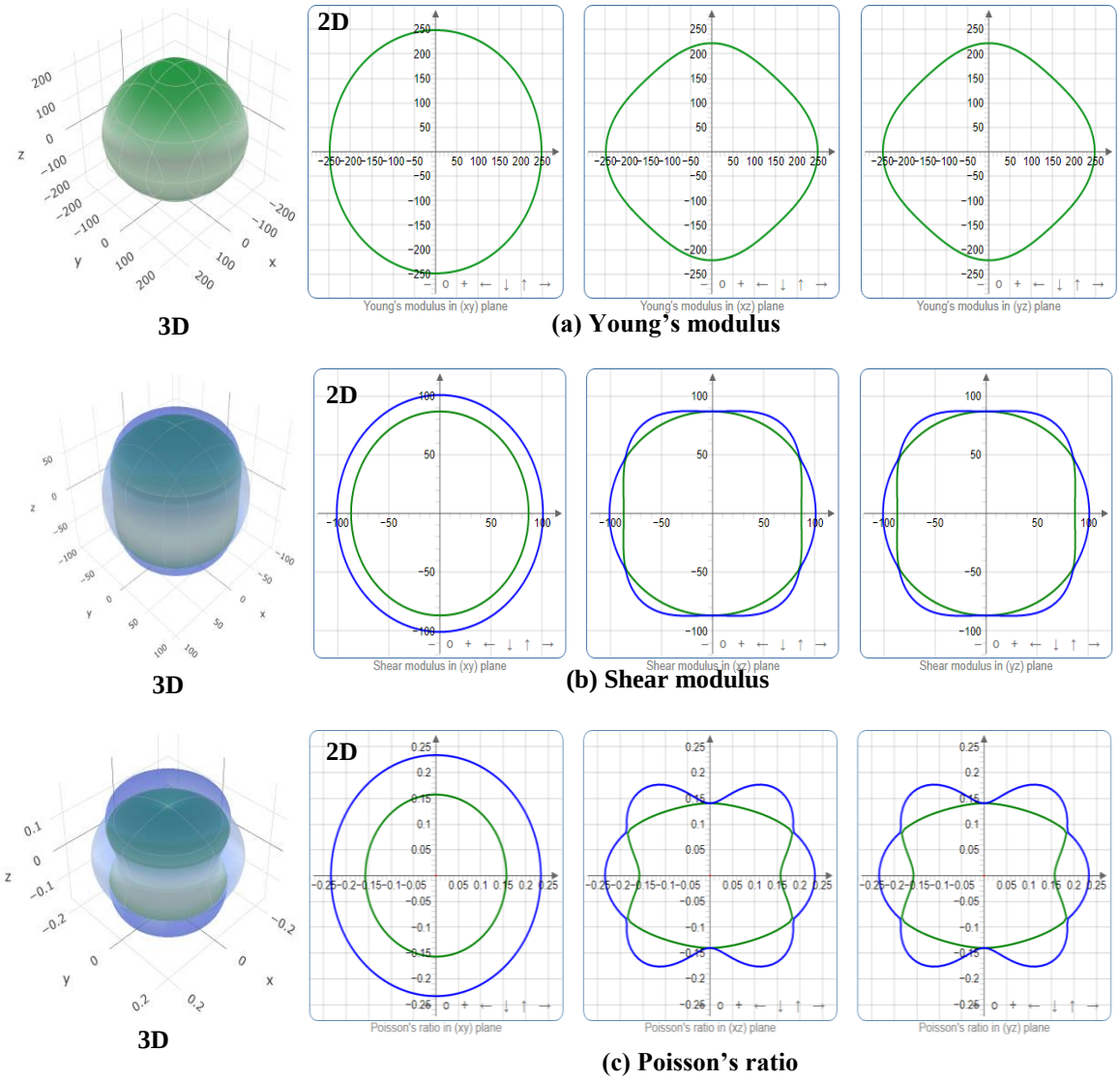

Fig. 4.3: Shows contour (3D) and two-dimensional (2D) charts of the Ti_2TlC compound's Young's modulus (Y), shear modulus (G), and Poisson's ratio (ν).

Table 4.4 Lists the minimum and maximum values for the Young's, G, and Poisson's ratios of the compounds Ti_2TlC, Zr_2TlC, and Hf_2TlC.

Phases	Y_{min}	Y_{max}	Y_{max}/Y_{min}	G_{min}	G_{max}	G_{max}/G_{min}	υ_{mn}	υ_{max}	$\upsilon_{max}/\upsilon_{min}$
Ti_2TlC	211	248	1.18	87	102	1.17	0.14	0.23	1.64
Zr_2TlC	202	228	1.13	81	92	1.14	0.21	0.27	1.29
Hf_2TlC	258	292	1.13	102	121	1.19	0.20	0.28	1.4

To understand hardness of studied compounds, we have calculated two parameters like as micro and macro-hardness following the relations: $H_{micro} = \frac{(1-2\nu)E}{6(1+\nu)}$[22] and $H_{macro} = 2[\left(\frac{G}{B}\right)^2 G]^{0.585} - 3$ [26]. It is seen that Ti_2TlC exhibits much higher and greater for H_{micro} (24 GPa) and H_{macro} (17 GPa) than that of Zr_2TlC (17 and 13 GPa) and Hf_2TlC (20 and 16 GPa), respectively. We can compare the hardiness of studied compounds such a way for both hardness Ti_2TlC > Hf_2TlC > Zr_2TlC. The lower Poisson ratio of Ti_2TlC impacts on higher hardness, however Young modulus of Hf_2TlC is greater than Ti_2TlC. The Mulliken bond populations has been considered to calculate Vickers hardness (H_v) [14,58] and presented those in Table 4.5.

$$H_V = \left[\prod^{\mu}\left\{740\left(P^{\mu} - P^{\mu'}\right)\left(v_b^{\mu}\right)^{-5/3}\right\}^{n^{\mu}}\right]^{1/\sum n^{\mu}}$$

Where P^{μ} is the Mulliken population of the μ-type bond, $P^{\mu'} = n_{free}/V$ is the metallic population, and v_b^{μ} is the bond volume of μ-type bond. The values are determined to be 2.18, 1.61 and 2.60 GPa for the phases Ti_2TlC, Zr_2TlC and Hf_2TlC compounds, respectively. The Hf_2TlC shows higher than Ti_2TlC and Zr_2TlC phases that are due to maximum elastic moduli. The measured hardness values correspond to well-known

MAX phase nanolaminates (in the 2 - 8 GPa range), including Hf_2InC (3.45 GPa) and Ta_2InC (4.12 GPa) [59].

Table 4.5. Calculated Mulliken populations [μ-type bond P^{μ}, bond length d^{μ}(Å) metallic population $P^{\mu'}$, bond volume v_b^{μ} (Å^3),Vicker's hardness of μ-type bond H_V^{μ} (GPa) and H_V (GPa)] of Ti_2TlC, Zr_2TlC and Hf_2TlC.

Phases	Bond	d^{μ}	P^{μ}	$P^{\mu'}$	v_b^{μ}	H_V^{μ}	H_V
Ti_2TlC	C-Ti	2.14	0.99	0.085	31.04	2.18	2.18
Zr_2TlC	C-Zr	2.30	1.00	0.077	37.69	1.61	1.61
Hf_2TlC	C-Hf	2.31	1.45	0.022	36.81	2.60	2.60

4.4 Electronic properties

4.4.1 Band structure and density of states (DOS)

Ti_2TlC, Zr_2TlC, and Hf_2TlC are examples of M_2TlC compounds with high-symmetry k points. The electronic energy band structures of these compounds are depicted in Fig. 4.4(a),(b),and(c), respectively. Since the compounds' conduction bands (red colors) span the E_F line (dashed black line) and noticeably overlap the valence bands (blue lines) (black colors), no band gap is observed, demonstrating the compounds' metallic character. Many strongly dispersive bands have been identified at and around the E_F for the phases Zr_2TlC and Hf_2TlC. (Fig. 4.4 b,c). Nonetheless, a complicated hybrid band character has been observed, comprising the quasi-flat band for the Ti_2TlC combination (Fig. 4.4a) and several low dispersive bands crossing the E_F. The electrical conductivity should be lower in the c direction in contrast to the ab plane (axis), according to the energy band structure, because there is less energy dispersion there.

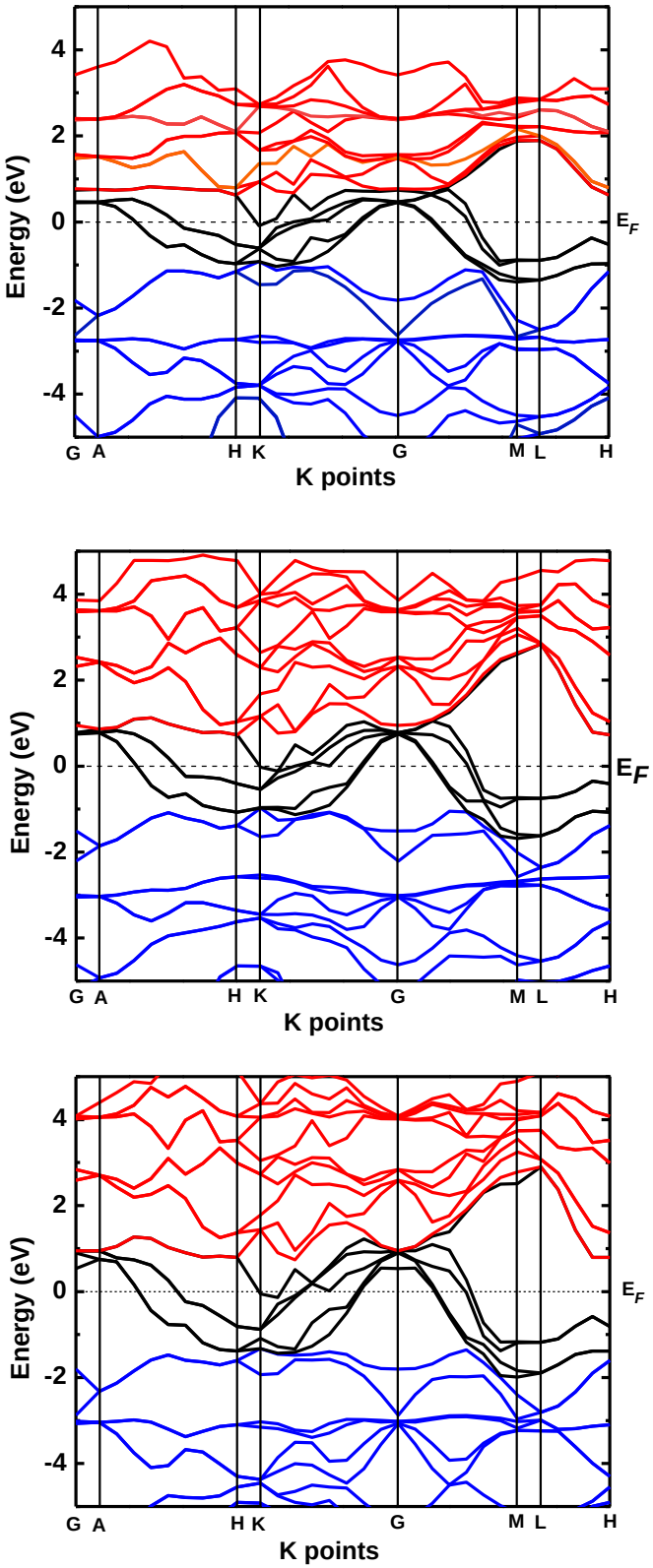

Fig. 4.4: Band structures of M_2TlC (a) Ti_2TlC (b) Zr_2TlC, and (c) Hf_2TlC.

Understanding band structure topographies requires an awareness of both the complete and partial densities of entities. The computed total density of state (TDOS) and partial density of state (PDOS) of the M_2TlC phases (Ti_2TlC, Zr_2TlC, and Hf_2TlC) are shown in Figs. 4.5(a) through (c), where the vertically broken line denotes the Fermi level, E_F. Three sub-bands can be separated out of the valence band. The Ti-3d, C-2p [for the Ti_2TlC phase], Zr-4d, C-2p [for the Zr_2TlC phase], and Hf-5p, 5d, C-2p [for the Hf_2TlC phase] states are the principal sources of the minimum energy sub-band (-6 eV to -2 eV).

Broad nature's middle sub-band (-2 - 0 eV) is mostly produced by the contributions due to Ti-3*p*, Ti-3*d*, Tl-6*p* [for Ti_2TlC phase], Zr-4*d*, Zr-4*p*, Tl-6*p* [for Zr_2TlC phase], Hf-5*p*,Hf-5*d* , Tl-6*p* [for Hf_2TlC phase]. The upper sub-band (0 - +6 eV) is formed by the aids of orbitals due to Ti-3*d*, Tl-6*s*, 6*p* [for Ti_2TlC phase], Zr-4*d*, Tl-6*s*, 6*p* [for Zr_2TlC phase], Hf-6*s*, 5*p*, 5*d* , Tl-6*s*, 6*p*[for Hf_2TlC phase]. The sub-band crossing the E_F (black colors in Fig. 4.5a,b,c) is resulting mainly from Ti-3*d*, Zr-4*d*, Hf-5*p*, 5*d* and Tl-6*p* electronic orbitals that are contributed strongly in the electronic conduction and significantly affect the physical properties of the phases. The value of DOS at E_F estimates and observed to be 3.0, 2.55 and 2.09 states/eV (Fig. 4.5a,b.c) for Ti_2TlC, Zr_2TlC, and Hf_2TlC phases, respectively.

Six bands are firmly mixed and cross the E_F during the phase Hf_2TlC, however four bands have crossed the E_F for Ti_2TlC and Zr_2TlC, therefore maximum findings of Vickers hardness are predicted for Ti_2TlC and Zr_2TlC phases comparing with Hf_2TlC phase.

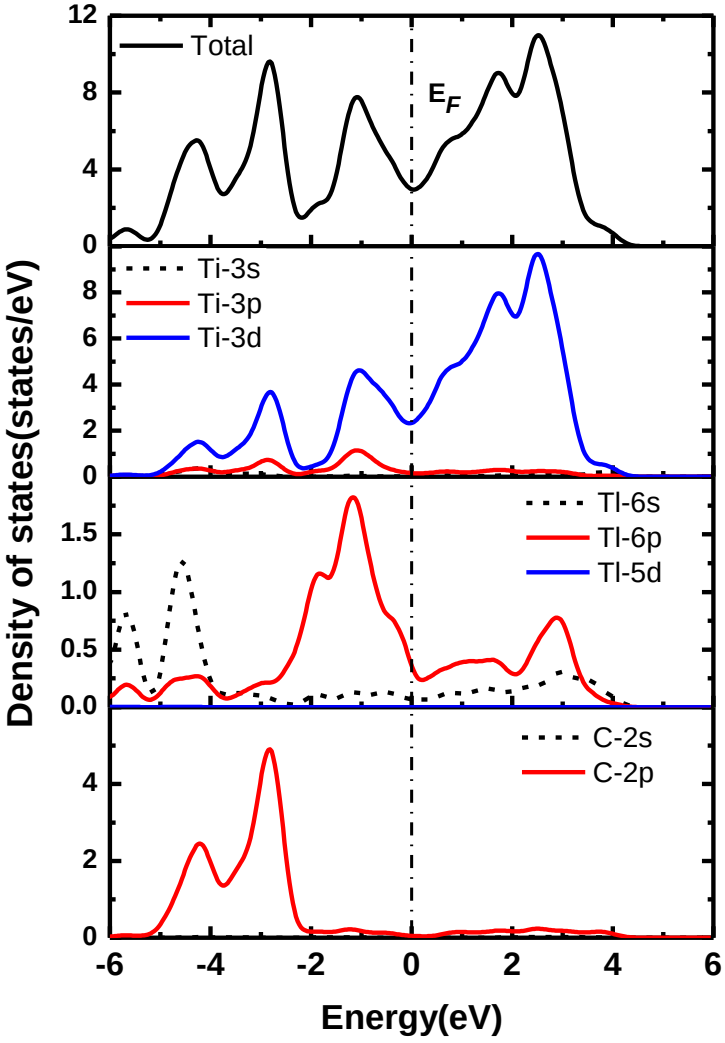

Fig. 4.5 (a): The total and partial density of states (TDOS and PDOS) of Ti_2TlC

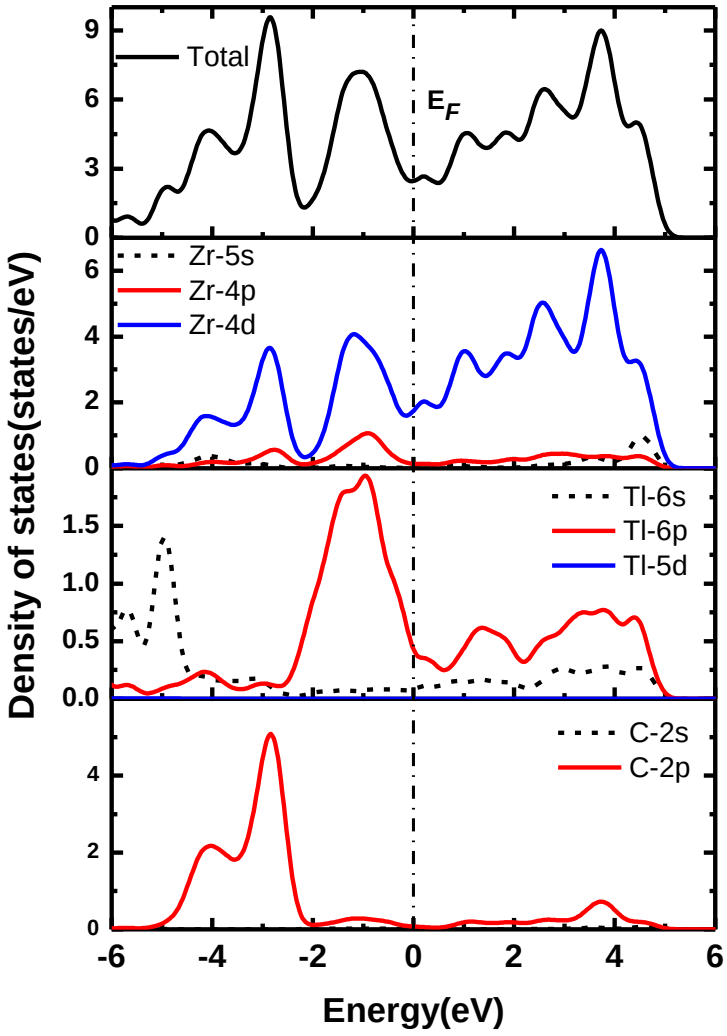

Fig. 4.5 (b): The TDOS and PDOS of Zr_2TlC

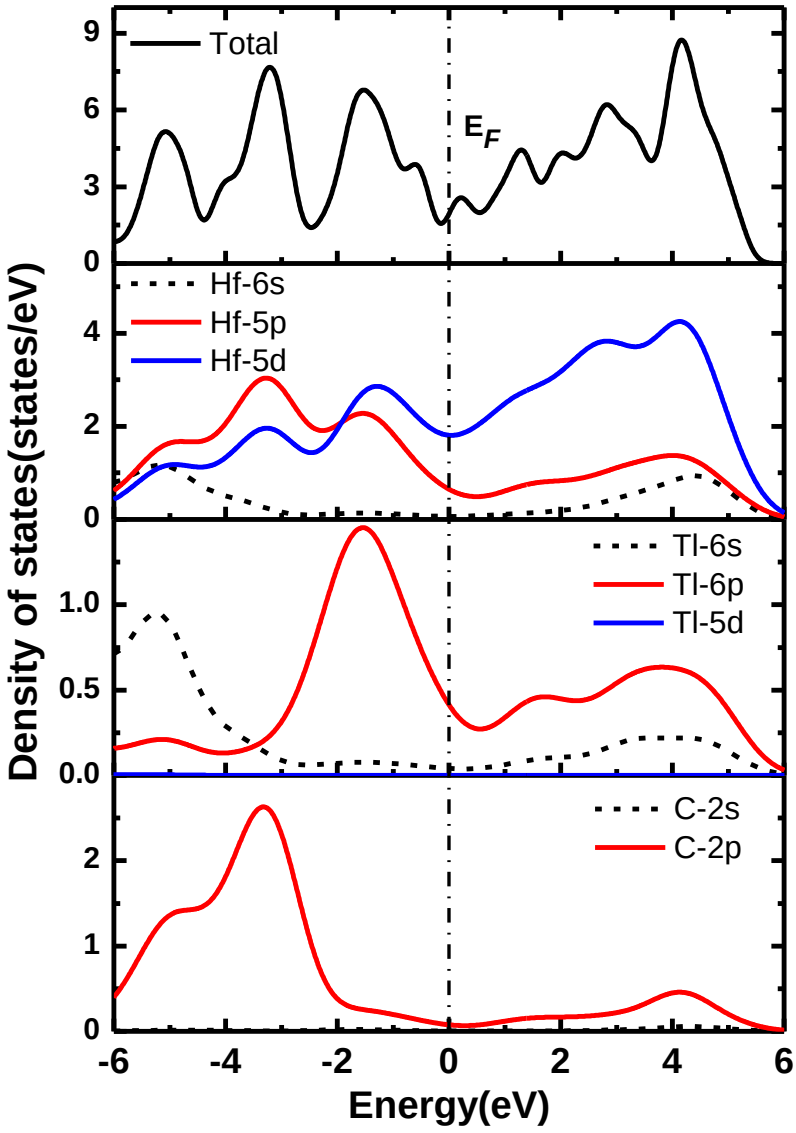

Fig. 4.5 (c): The TDOS and PDOS of Hf_2TlC

4.4.2 Mulliken populations study

The Mulliken atomic population (MAP) analyzes the EVC (Effective Valence Charge) and their formalism is described elsewhere [18]. The effective valence charge in a crystal refers to the distinction from the formal ionic charge and the Mulliken charge. Whether the bonds are ionic or covalent is shown by the value of EVC. When the values of EVC is zero (positive), the bond is ideal ionic in nature; nevertheless, when it deviates from zero, it displays the level of covalency. The computed EVC is shown in Table 4.6, that shows there is significant covalency in chemical bonding within the investigated compounds [17,58,59].

Table 4.6. Mulliken atomic populations of Ti_2TlC, Zr_2TlC and Hf_2TlC compounds.

Mulliken atomic population							
Phases	Atoms	*s*	*p*	*d*	Total	Charge (e)	EVC (e)
	C	1.47	3.29	0.00	4.76	-0.76	4.76
Ti_2TlC	Ti	2.22	6.72	2.64	11.59	0.41	11.59
	Tl	1.14	1.89	10.02	13.06	-0.06	13.06
	C	1.48	3.31	0.00	4.80	-0.80	4.80
Zr_2TlC	Zr	2.26	6.61	2.67	11.54	0.46	11.54
	Tl	1.19	1.90	10.02	13.12	-0.12	13.12
	C	1.54	3.35	0.00	4.89	-0.89	4.89
Hf_2TlC	Hf	0.46	0.44	2.76	3.66	0.34	3.66
	Tl	0.79	1.98	10.02	12.79	0.21	12.79

The findings of the bond of population (BOP) are interpreted: The electronic populations of two atoms interact insignificantly, hence the hardness calculation is omitted; i) Positive: Atoms near one another form bonds; ii) Negative: Atoms near one

another form anti-bonds. Bonds with a maximum BOP value have a high level of covalency. The bond Hf-C in the compounds under study has the highest covalency of all the bonds. Additionally, the Hf_2TlC has a stronger overall bond than Ti_2TlC and Zr_2TlC. As shown in Table 4.5. It is therefore expected that this compound's hardness value is higher than that of the other. The well-known atomic population analysis can also be used to understand how charges move between atoms. For instance, in Ti_2TlC, charge transfers with values of 0.76e and 0.06e, respectively, from Ti to C and Tl. There are more compounds with comparable phase show topographies.

4.5 Optical properties

When electromagnetic fields with the appropriate energy are applied to occupied stage (lower the E_F) and unoccupied stages, electronic transitions take place (above the E_F). As a result, in metal and systems of a similar kind, intra-band and interband contributions, having the latter arriving from the lower energy infrared portion of the spectra, account for the majority of the optical feature of the solids.

The dielectric capability is calculated using the following variables: 3 eV plasma frequencies; 0.05 eV damping [59,60]. Zr_2TlC, Ti_2TlC and Hf_2TlC compounds' optical characteristics can be estimated using frequency-dependent dielectric function. The fictitious component $\varepsilon_2(\omega)$ of the dielectric function $\varepsilon(\omega)$ is calculated using the momentum matrix elements from the inhabited and uninhabited electronic stages and is given by [61].

$$\varepsilon_2(\omega) = \frac{2e^2\pi}{\Omega\varepsilon_0} \sum_{k,v,c} \left|\psi_k^c \left|\boldsymbol{u}.\boldsymbol{r}\right|\psi_k^v\right|^2 \delta\left(E_k^c - E_k^v - E\right)$$

Here, ω is the light frequency, u is the vector representing the polarization of the input electric field, e is the electronic charge, and ψ_k^c is the conduction band wave function at

k and ψ_k^v is valence band wave function at k, respectively. The Kramers-Kronig equation, which links the real and imaginary parts, may be used to compute the dielectric function's (ε_1) real portion.

Ti_2TlC, Zr_2TlC, and Hf_2TlC have had their optical characteristics estimated for photon energies between polarization vectors of the electric field up to 20 eV between [100] and [001]. An observation is made where optical spectra to these polarization directions are comparable and nearly identical. As a result, data along [100] direction are provided in Figs 4.6 (a to h).

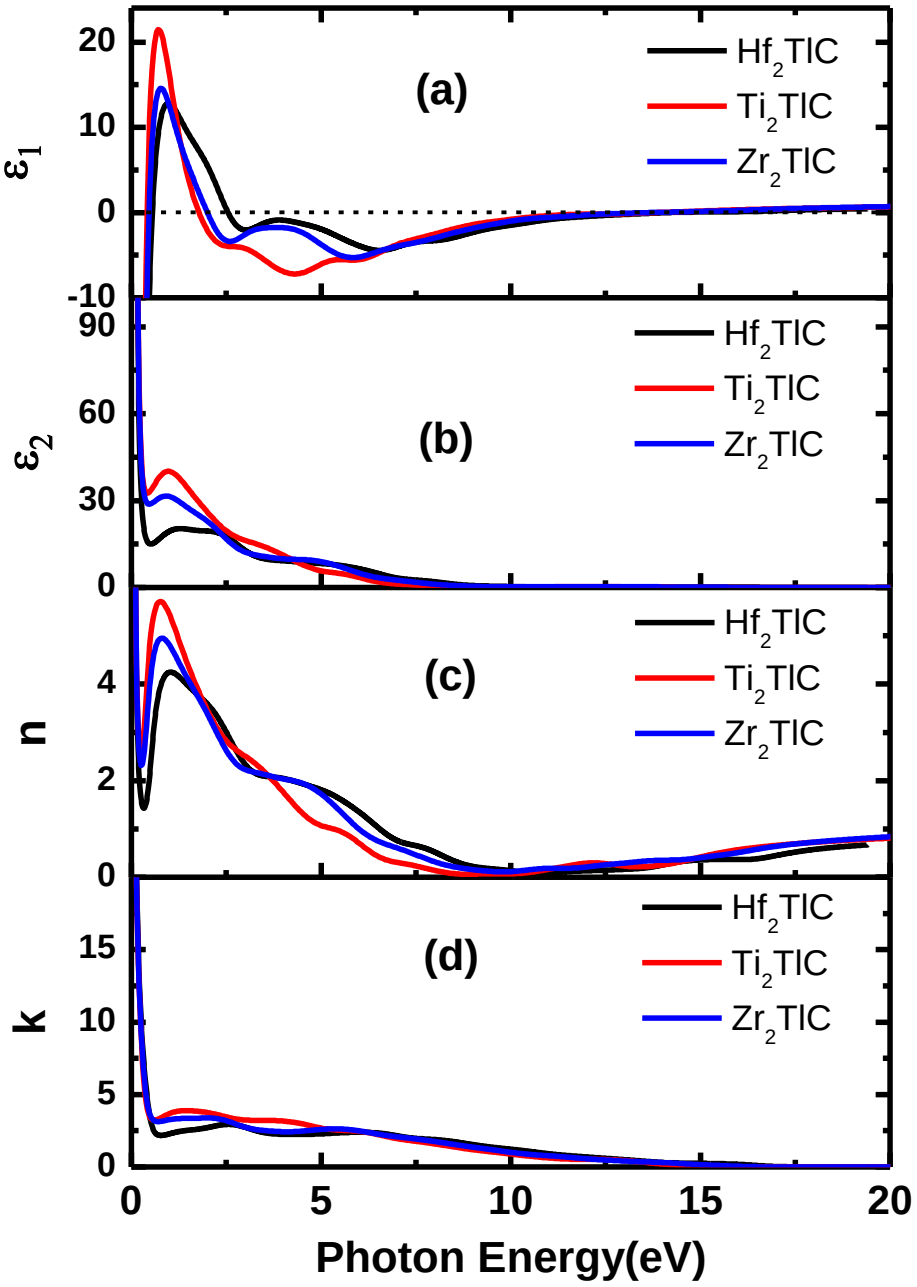

Fig. 4.6 (a-d): Dielectric function energy dependency actual part, imaginary part, refractive index, extinction coefficient, respectively of the Ti_2TlC, Zr_2TlC, and Hf_2TlC compounds for [100] electric field polarization.

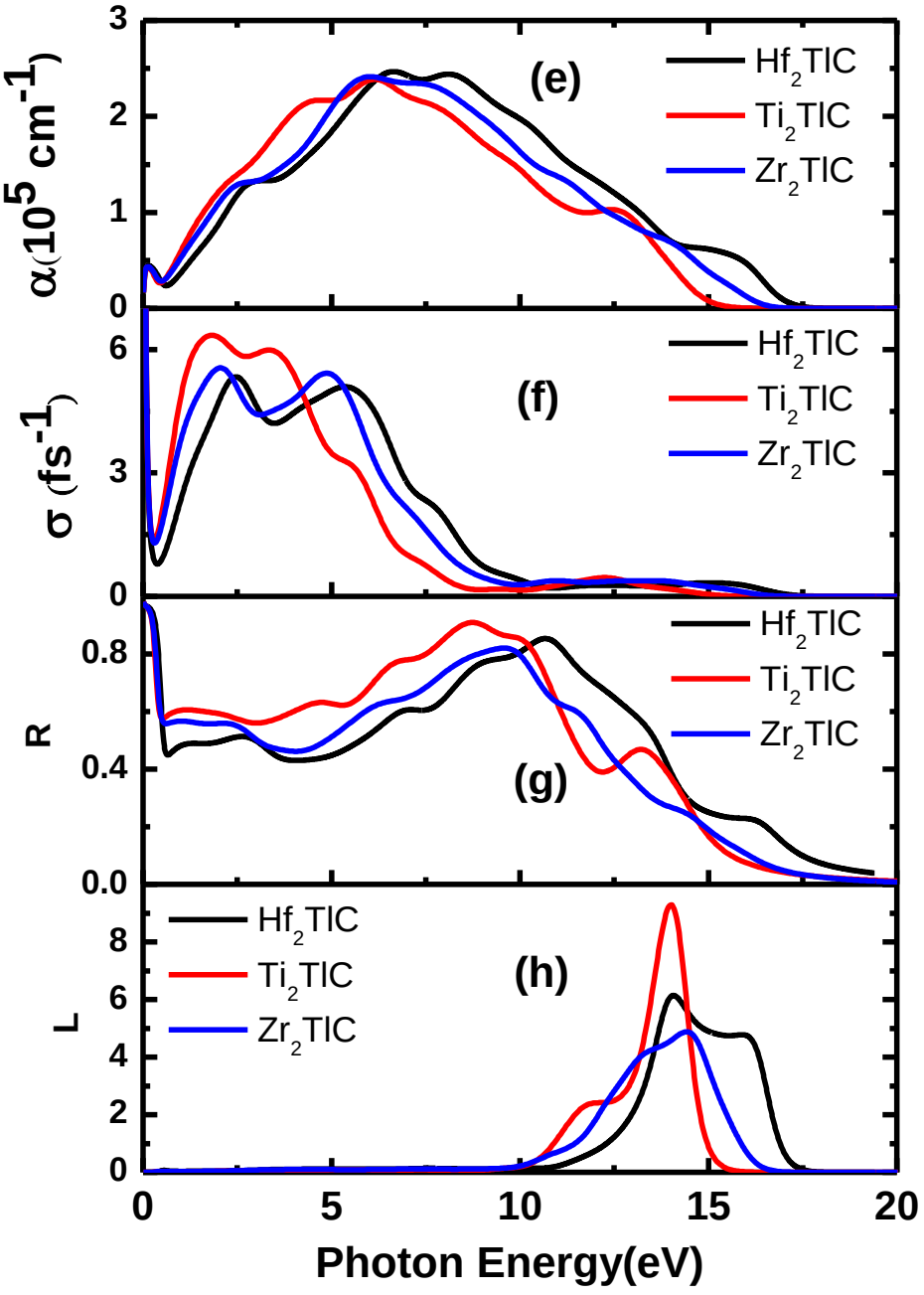

Fig. 4.6 (e-h): (e) absorption coefficient, (f) photo conductivity, (g) reflectivity, and (h) loss function of the Ti_2TlC, Zr_2TlC, and Hf_2TlC compounds, respectively for [100] electric field polarization

Figure 4.6a illustrates the actual portion of the dielectric function, ε_1, for the phases Ti_2TlC, Zr_2TlC, and Hf_2TlC. The optical characteristics of the materials have been greatly influenced by the intra-band transition of electrons, which mostly affects the infrared spectrum's low energy area. The intraband transition of electrons causes the minimum energy peaks, which are measured to be at 0.72, 0.76, and 0.96 eV in the ε_1 curves for the Ti_2TlC, Zr_2TlC, and Hf_2TlC phases, respectively. For the materials that suggest a Drude-like behavior, the (ε_1) exhibits higher negative values, which correlates to our conversation in section 3.3. Fig. 4.6b shows the compounds' hypothetical portion, or ε_2. For the compounds Ti_2TlC, Zr_2TlC, and Hf_2TlC, respectively, the ε_1 depicts zero value from below at approximately 14.0, 14.5, and 13.8 eV (Fig. 4.6a), and the ε_2 approaches zero from above at approximately 9.96, 9.93, and 10.75 eV (Fig. 4.6b), further stating the metallic nature of the studied phases.

Figure 4.6. depicts the phases' computed frequency-dependent refractive index and extinction coefficient (c,d). In the design of optoelectronic components, a material's high value of n is crucial. The primary peaks for the phases Ti_2TlC, Zr_2TlC, and Hf_2TlC, respectively, are determine to be at 0.76, 0.80, and 0.96 eV for the static values of n(0), which are determined to be 20.8, 20.87, and 19.8. The relationship between the extinction and absorption coefficients is given by $k(\alpha = 4\pi k/\lambda)$. For Ti_2TlC, Zr_2TlC, and Hf_2TlC, the sharp peaks were found at 1.45, 2.0, and 2.5 eV, respectively. The intra-band transitions of electrons define these peaks (Fig.4.6d).

The energy that the electron must absorb to excite as a result of light passing through the materials is represented by the absorption coefficient. A calculation of the absorption coefficient (α) energy dependence is shown in Fig. 4.6. (e). In the ultraviolet

(UV) region, the value of is strong, whereas it is weak in the IR (infrared) spectrum. The value of increases steadily as photon energy rises in the direction of the UV area, peaking at 6.1, 5.9, and 6.6 eV for the compounds Ti_2TlC, Zr_2TlC, and Hf_2TlC, respectively. The fact that it has a high value throughout a huge energy range implies, which might be employed in optoelectronic equipment that function in the visible and ultraviolet light spectrums. Because the studied compounds are metallic, their photoconductivity begins at zero photon energy (see Fig. 4.6f).

The Ti_2TlC substance has maximum photo-conductivity at 1.81 eV, while the maxima for other compounds were 2.02 eV (Zr_2TlC) and 2.45 eV, respectively (Hf_2TlC). The compounds' photon energy-dependent reflectivity (R) spectra are as seen in Fig. 4.6g. As can be observed, the value of R starts out at 97% for all phases and increases to high values of 92%, 82%, and 86% for the compounds Ti_2TlC, Zr_2TlC, and Hf_2TlC, respectively, at 8.76 eV, 9.6 eV, and 10.7 eV. A compound with a reflectivity of 44% in the visible light band is reported to be able to reduce solar heating, according to sources [62]. The reflectivity is always over 44% for the phases Ti_2TlC (11.67 eV), Zr_2TlC (12.44 eV), and Hf_2TlC (13.8 eV) beyond they are not maintained, which is an interesting observation. The results of R indicate that the visible (1.7 eV - 3.3 eV) and IR (1.24 meV to 1.7 eV) regions cover energy over 44% up to 12.0 eV. The studied compounds may therefore be a strong candidate for utilize as a covering material to lessen solar heating. The reflectance spectra of all phases strategy zero when the input photon energy is about 20 eV.

The loss spectrum (L), which may also be interpreted using the dielectric function, is defined as the amount of energy lost by the photon during light transmission through the materials. Figure 4.6h depicts estimated values for L for each phase. Up to 10 eV, none of the examined chemicals exhibit any loss. In the 14–14.5 eV energy range, the loss peaks were discovered.

The peaks are more pronounced in the energy region between 0 and 1 where the dielectric function occurs. The plasma frequency, ω_P, which is determined to be at 14.0, 14.0, and 14.5 eV for the substances Ti_2TlC, Zr_2TlC, and Hf_2TlC, respectively, is linked to the loss peaks.

5 Conclusions

5.1 General

The ternary carbides M_2TlC (M = Ti, Zr, Hf) MAX phases' dynamical stability, thermodynamics, and optical characteristics have been thoroughly examined. In addition, the compounds' new additional data on elastic, Mulliken analysis, and Vickers hardness is taken into consideration while reviewing the compounds' structural and electrical properties.

5.2 Key findings

The following concluding remarks provide a summary of the acquired results:

To evaluate the accuracy of our computations, the compounds' structural, elastic, and electrical properties are reviewed. The examined lattice parameters, elastic constants, and C_{ij}, such as the polycrystalline elastic constants, were consistent with previous findings and fulfilled the traditional mechanical stability requirements. The ratios Pugh and Poisson support the brittleness of the compounds found in nature. Calculations and analyses have been done on the electronic band formation, DOS, Mulliken atomic, electron charge density locating and bond overlap populations. Since Ti_2TlC has greater elastic moduli than the other compounds tested, it exhibits a higher anisotropic index than the others. Since the valence and conduction bands overlap with E_F, no band gap to be seen, that means the compounds are metallic. The examined phases' electronic orbitals Ti-3d, Zr-4d, Hf-5p, 5d, and Tl-6p considerably contribute to the electronic conduction that affects the physical properties. For the phases, the findings of DOS at E_F were discovered to be 3.0, 2.55, and 2.09 states per eV. These strong covalent bonds are raised from the best hybridization of Ti-3d, Zr-4d, and Hf-5d with Tl-6p and C-2p electrons at the Fermi level. The phases of

Ti_2TlC, Zr_2TlC, and Hf_2TlC compounds, respectively, have Vicker's hardness values of 2.18, 1.61, and 2.60 GPa, indicating a moderately hard nature to the materials. The phonon dispersion curves show no evidence of negative frequency, and as a result, the examined substances are assumed to be dynamically stable. The static values of n(0) are determined to be 20.8, 20.87, and 19.8, respectively, with the primary peaks for the phases Ti_2TlC, Zr_2TlC, and Hf_2TlC emerging at 0.76, 0.80, and 0.96 eV, suggesting that the materials might be utilized to create optoelectronic appliances. The values of R reveal that the visible and IR regions (1.24 eV–1.7 eV) cover above 40% of the energy up to 12.0 eV. (1.7 eV – 3.3 eV).

5.3 Practical implication

The investigated compounds M_2TlC (M = Ti, Zr, Hf) represent a promising possibility for actual application as a covering material to lessen solar heating.

5.4 Suggestions for further research work

To implement these MAX phases compounds M_2TlC (M = Ti, Zr, Hf) needs comprehensive study on transport properties with along micro hardness study. For time constrain, we could not study these interesting phenomena. There is a room to study that topics and to proceed implementation of ternary carbide M_2InC in optoelectronic and industrial applications.

Bibliography

[1] M.W. Barsoum, G. Yaroschuk, S. Tyagi, Fabrication and characterization of M2SnC (M= Ti, Zr, Hf and Nb), Scripta Materialia. 37 (1997) 1583–1591.

[2] V.H. Nowotny, Strukturchemie einiger verbindungen der übergangsmetalle mit den elementen C, Si, Ge, Sn, Progress in Solid State Chemistry. 5 (1971) 27–70.

[3] M.W. Barsoum, The MN+ 1AXN phases: A new class of solids: Thermodynamically stable nanolaminates, Progress in Solid State Chemistry. 28 (2000) 201–281.

[4] M.W. Barsoum, MAX phases: Properties of machinable ternary carbides and nitrides, 2013. https://doi.org/10.1002/9783527654581.

[5] M. Naguib, G.W. Bentzel, J. Shah, J. Halim, E.N. Caspi, J. Lu, L. Hultman, M.W. Barsoum, New solid solution MAX phases: (Ti0.5, V0.5)3AlC2, (Nb0.5, V0.5)2AlC, (Nb0.5, V0.5)4AlC3 and (Nb0.8, Zr0.2)2AlC, Materials Research Letters. 2 (2014) 233–240. https://doi.org/10.1080/21663831.2014.932858.

[6] D. Horlait, S. Grasso, A. Chroneos, W.E. Lee, Attempts to synthesise quaternary MAX phases (Zr,m)2ALC and Zr2(AL,A)C as a way to approach Zr2ALC, Materials Research Letters. 4 (2016) 137–144. https://doi.org/10.1080/21663831.2016.1143053.

[7] M.W. Barsoum, The M ,, AXN Phases : A New Class of Solids ;, 28 (2000) 201–281.

[8] B. Anasori, J. Halim, J. Lu, C.A. Voigt, L. Hultman, M.W. Barsoum, Mo2TiAlC2: A new ordered layered ternary carbide, Scripta Materialia. 101 (2015) 5–7.

[9] E.N. Caspi, P. Chartier, F. Porcher, F. Damay, T. Cabioc, Ordering of (Cr , V) Layers in Nanolamellar (Cr 0 . 5 V 0 . 5) n, (2015). https://doi.org/10.1080/21663831.2014.975294.

[10] R. Meshkian, Q. Tao, M. Dahlqvist, J. Lu, L. Hultman, Theoretical stability and materials synthesis of a chemically ordered MAX phase , Mo2ScAlC2 , and its two-dimensional derivate Mo2ScC2 MXene, 125 (2017) 476–480.

[11] D. Horlait, S.C. Middleburgh, A. Chroneos, W.E. Lee, Synthesis and DFT investigation of new bismuth-containing MAX phases, Nature Publishing Group. (2016) 1–9. https://doi.org/10.1038/srep18829.

[12] D. Horlait, S. Grasso, N. Al Nasiri, P.A. Burr, W.E. Lee, Synthesis and oxidation testing of MAX phase composites in the Cr–Ti–Al–C quaternary system, Journal of the American Ceramic Society. 99 (2016) 682–690.

[13] T. Lapauw, K. Lambrinou, T. Cabioch, J. Halim, J. Lu, A. Pesach, O. Rivin, O. Ozeri, E.N. Caspi, L. Hultman, P. Eklund, J. Rosén, M. Barsoum, J. Vleugels, T. Lapauw, K. Lambrinou, T. Cabioch, J. Halim, J. Lu, A. Pesach, O. Rivin, O. Ozeri, E.N. Caspi, L. Hultman, P. Eklund, J. Rosén, M. Barsoum, J. Vleugels, Synthesis of the new MAX phase Zr2AlC, (2016) 1847–1853.

[14] F. Sultana, M.M. Uddin, M.A. Ali, M.M. Hossain, S.H. Naqib, A.K.M.A. Islam, First principles study of M2InC (M = Zr, Hf and Ta) MAX phases: The effect of M atomic species, Results in Physics. 11 (2018) 869–876. https://doi.org/10.1016/J.RINP.2018.10.044.

[15] M.A. Ali, M.S. Ali, M.M. Uddin, Structural, elastic, electronic and optical properties of metastable MAX phase Ti5SiC4 compound, Indian Journal of Pure and Applied Physics. 54 (2016) 386–390.

[16] M. Roknuzzaman, M.A. Hadi, M.A. Ali, M.M. Hossain, N. Jahan, M.M. Uddin, J.A. Alarco, K. Ostrikov, First hafnium-based MAX phase in the 312 family, Hf3AlC2: A

first-principles study, Journal of Alloys and Compounds. 727 (2017) 616–626.

[17] M.A. Ali, M.M. Hossain, M.A. Hossain, M.T. Nasir, M.M. Uddin, M.Z. Hasan, A. Islam, S.H. Naqib, Recently synthesized (Zr1-xTix) 2AlC (0≤ x≤ 1) solid solutions: Theoretical study of the effects of M mixing on physical properties, Journal of Alloys and Compounds. 743 (2018) 146–154.

[18] A. Chowdhury, M.A. Ali, M.M. Hossain, M.M. Uddin, S.H. Naqib, A. Islam, Predicted MAX phase Sc2InC: dynamical stability, vibrational and optical properties, Physica Status Solidi (B). 255 (2018) 1700235.

[19] B. Anasori, Û.G. Gogotsi, 2D metal carbides and nitrides (MXenes), Springer, 2019.

[20] V.N. Naguib, M.W. Mochalin, Barsoum, and Y. Gogotsi, Adv. Mater. 26 (2014) 992.

[21] K. Das, M.A. Ali, M.M. Hossain, S.H. Naqib, A.K.M.A. Islam, M.M. Uddin, Dynamical stability , Vibrational and optical properties of anti-perovskite A 3 BX (Ti 3 TlN , Ni 3 SnN and Co 3 AlC) phases : a first principles study, (n.d.).

[22] A. Bouhemadou, Structural, electronic and elastic properties of Ti2TlC, Zr2TlC and Hf2TlC, Central European Journal of Physics. 7 (2009) 753–761. https://doi.org/10.2478/s11534-009-0022-z.

[23] J.A. Warner, S.K.R. Patil, S. V Khare, K.C. Masiulaniec, Ab initio calculations for properties of MAX phases Ti 2 Tl C, Zr 2 Tl C, and Hf 2 Tl C, Applied Physics Letters. 88 (2006) 101911.

[24] D. YL, S. ZM, H. Hashimoto, T. WB, First-principles study on thermodynamic properties of Ti2AlC and Ti2SC, Materials Transactions. 50 (2009) 2173–2176.

[25] A.H. Reshak, Z. Charifi, H. Baaziz, The effect of the phase transition on the optical properties of the lanthanum monopnictide compounds, Journal of Physics: Condensed Matter. 20 (2008) 325207.

[26] M. Xu, S. Wang, G. Yin, J. Li, Y. Zheng, L. Chen, Y. Jia, Optical properties of cubic Ti 3 N 4, Zr 3 N 4, and Hf 3 N 4, Applied Physics Letters. 89 (2006) 151908.

[27] A. Bouhemadou, R. Khenata, M. Kharoubi, Y. Medkour, First-principles study of structural and elastic properties of Sc2AC (A= Al, Ga, In, Tl), Solid State Communications. 146 (2008) 175–180.

[28] M.F. Cover, O. Warschkow, M.M.M. Bilek, D.R. McKenzie, A comprehensive survey of M2AX phase elastic properties, Journal of Physics: Condensed Matter. 21 (2009) 305403.

[29] D. Music, Z. Sun, J.M. Schneider, Electronic structure of Sc2AC (A= Al, Ga, In, Tl), Solid State Communications. 133 (2005) 381–383.

[30] S. Gupta, E.N. Hoffman, M.W. Barsoum, Synthesis and oxidation of Ti2InC, Zr2InC, (Ti0.5,Zr0.5)2InC and (Ti0.5,Hf0.5)2InC in air, Journal of Alloys and Compounds. 426 (2006) 168–175. https://doi.org/10.1016/J.JALLCOM.2006.02.049.

[31] B. Manoun, C.S. Zha, Compression behavior of M 2 AlC (M = Ti , V , Cr , Nb , and Ta) phases to above 50 GPa, (2006) 1–7. https://doi.org/10.1103/PhysRevB.73.024110.

[32] M.W. Barsoum, I. Salama, T. El-Raghy, J. Golczewski, H.J. Seifert, F. Aldinger, W.D. Porter, H. Wang, Thermal and electrical properties of Nb 2 AlC,(Ti, Nb) 2 AlC and Ti 2 AlC, Metallurgical and Materials Transactions A. 33 (2002) 2775–2779.

[33] X. He, Y. Bai, Y. Li, C. Zhu, M. Li, Ab initio calculations for properties of MAX phases Ti2InC, Zr2InC, and Hf2InC, Solid State Communications. 149 (2009) 564–566. https://doi.org/10.1016/j.ssc.2008.12.047.

[34] H. Bolvardi, J. Emmerlich, M. to Baben, D. Music, J. von Appen, R. Dronskowski, J.M. Schneider, Systematic study on the electronic structure and mechanical properties of X_2 BC (X = Mo, Ti, V, Zr, Nb, Hf, Ta and W), Journal of Physics: Condensed Matter. 25 (2013) 045501. https://doi.org/10.1088/0953-8984/25/4/045501.

[35] M.D. Segall, P.J.D. Lindan, M.J. al Probert, C.J. Pickard, P.J. Hasnip, S.J. Clark, M.C. Payne, First-principles simulation: ideas, illustrations and the CASTEP code, Journal of Physics: Condensed Matter. 14 (2002) 2717.

[36] S. Baroni, S. De Gironcoli, A. Dal Corso, P. Giannozzi, Phonons and related crystal properties from density-functional perturbation theory, Reviews of Modern Physics. 73 (2001) 515.

[37] [Cramer; J., No Title, 2002. https://www.wiley.com/en-us/Essentials+of+Computational+Chemistry:+Theories+and+Models,+2nd+Edition-p-9780470091821.

[38] F. Jensen, No Title, (2007) 98–149. https://www.wiley.com/en-us/Introduction+to+Computational+Chemistry%2C+3rd+Edition-p-9781118825990.

[39] D.R. Hartree, No Title, (1928) 426. https://www.scirp.org/(S(lz5mqp453edsnp55rrgjct55))/reference/ReferencesPapers.aspx?ReferenceID=2093600.

[40] M. Segall, O. Limited, M. Probert, P.J. Hasnip, First-Principles Simulation : Ideas , Illustrations and the CASTEP Code First-principles simulation : ideas , illustrations and the CASTEP code, (2002). https://doi.org/10.1088/0953-8984/14/11/301.

[41] V. Singh, D. Joung, L. Zhai, S. Das, S.I. Khondaker, S. Seal, Graphene based materials: Past, present and future, Progress in Materials Science. 56 (2011). https://doi.org/10.1016/j.pmatsci.2011.03.003.

[42] G.P. FW Kutzler, No Title, Phys Rev B Condens Matter . (1992). https://pubmed.ncbi.nlm.nih.gov/10001891/.

[43] P. Durand, J.C. Barthelat, New atomic pseudopotentials for electronic structure calculations of molecules and solids, Chemical Physics Letters. 27 (1974) 191–194. https://doi.org/https://doi.org/10.1016/0009-2614(74)90201-2.

[44] M. Causà, Numerical Integration in Density Functional Methods with Linear Combination of Atomic Orbitals, in: C. Pisani (Ed.), Quantum-Mechanical Ab-Initio Calculation of the Properties of Crystalline Materials, Springer Berlin Heidelberg, Berlin, Heidelberg, 1996: pp. 91–100. https://doi.org/10.1007/978-3-642-61478-1_5.

[45] D.M. Ceperley, B.J. Alder, Ground state of the electron gas by a stochastic method, Physical Review Letters. 45 (1980) 566.

[46] D. Vanderbilt, Soft self-consistent pseudopotentials in a generalized eigenvalue formalism, Physical Review B. 41 (1990) 7892.

[47] H.J. Monkhorst, J.D. Pack, Special points for Brillouin-zone integrations, Physical Review B. 13 (1976) 5188.

[48] M.W. Barsoum, Physical properties of the MAX phases, Encyclopedia, Mater., Sci. Technol.. Amsterdam: Elsevier. (2006).

[49] F. Mouhat, F.-X. Coudert, Necessary and sufficient elastic stability conditions in various crystal systems, Physical Review B. 90 (2014) 224104.

[50] M. Zr, H. Max, P. An, M.W. Qureshi, X. Ma, G. Tang, R. Paudel, Structural Stability, Electronic, Mechanical, Phonon, and Thermodynamic Properties of the M 2 GaC (M = Zr, Hf) MAX Phase: An ab Initio Calculation, (2020).

[51] I.R. Shein, A.L. Ivanovskii, Elastic properties of superconducting MAX phases from first-principles calculations, Physica Status Solidi (B). 248 (2011) 228–232.

[52] W. Voigt, Lehrbuch der Kristallphysik, Lehrbuch Der Kristallphysik. (1966). https://doi.org/10.1007/978-3-663-15884-4.

[53] R. Hill, The elastic behaviour of a crystalline aggregate, Proceedings of the Physical Society. Section A. 65 (1952) 349.

[54] A. Reuß, Berechnung der fließgrenze von mischkristallen auf grund der plastizitätsbedingung für einkristalle., ZAMM-Journal of Applied Mathematics and Mechanics/Zeitschrift Für Angewandte Mathematik Und Mechanik. 9 (1929) 49–58.

[55] I.N. Frantsevich, F.F. Voronov, I.N. Frantsevich, Elastic Constants and Elastic Moduli of Metals and Insulators Handbook, (1983) 60–180.

[56] S.I. Ranganathan, M. Ostoja-Starzewski, Universal Elastic Anisotropy Index, Phys. Rev. Lett. 101 (2008) 55504. https://doi.org/10.1103/PhysRevLett.101.055504.

[57] R. Gaillac, P. Pullumbi, F.-X. Coudert, ELATE: an open-source online application for analysis and visualization of elastic tensors, Journal of Physics: Condensed Matter. 28 (2016) 275201.

[58] R.S. Mulliken, Electronic population analysis on LCAO–MO molecular wave functions. I, The Journal of Chemical Physics. 23 (1955) 1833–1840.

[59] T. Liao, J. Wang, Y. Zhou, Superior mechanical properties of Nb2AsC to those of other layered ternary carbides: a first-principles study, Journal of Physics: Condensed Matter. 18 (2006) L527.

[60] D.G. Pettifor, Theoretical predictions of structure and related properties of intermetallics, Materials Science and Technology. 8 (1992) 345–349.

[61] BIOVIA Material Studio, Castep Guide, BIOVIA Materials Studio 2020 Help. (2019). https://www-users.york.ac.uk/~mijp1/teaching/grad_FPMM/practical_classes/MS_CASTEP_guide.pdf.

[62] A.T. Petit, P.L. Dulong, Research on some important points of the theory of heat, Ann Chem Phys. 10 (1981) 395.

Impact of M atomic species on physical properties of M_2TlC (M = Ti, Zr, Hf): A first principles calculation

Cite as: AIP Advances 13, 065209 (2023); doi: 10.1063/5.0150252
Submitted: 13 March 2023 • Accepted: 22 May 2023 •
Published Online: 6 June 2023

M. Sohel,[1] M. M. Uddin,[1,a)] M. A. Ali,[1] M. M. Hossain,[1] A. K. M. A. Islam,[2,3] and S. H. Naqib[2]

AFFILIATIONS

[1] Department of Physics, Chittagong University of Engineering and Technology, Chattogram 4349, Bangladesh
[2] Department of Physics, University of Rajshahi, Rajshahi 6205, Bangladesh
[3] Department of Electrical and Electronic Engineering, International Islamic University Chittagong, Kumira, Chattogram 4318, Bangladesh

[a)] **Author to whom correspondence should be addressed:** mohi@cuet.ac.bd

ABSTRACT

We characterize the physical feature of M_2TlC (M = Ti, Zr, and Hf) MAX phase ternary carbides applying density functional theory. Along with previously calculated structural, elastic, and electrical properties, Vickers hardness, dynamical stability, and optical feature of the phases are also calculated. The Pugh ratio and Poisson's ratio show the compounds' brittleness in conjunction with their potent directional covalent bonds and combination of ionic contributions. The metallic character of the phases is supported by the Fermi level overlap of the conduction band and valence band. The examined materials have moderate hardness, according to the Vickers hardness, with the Hf_2TlC combination having the highest value of 2.60 GPa. A number of well-known phenomena are used to compute and thoroughly analyze the optical characteristics. Notably, all investigated compounds show reflectivity above 44% up to 12.0 eV energy, which is encompassed by the infrared and visible regions. The compounds could therefore be used, in practice, as a coating material to lessen solar heating.

I. INTRODUCTION

The study of MAX phases $M_{n+1}AX_n$ with n = 1–3, M = early transition metal; A = A-group elements from groups 12–16 in the Periodic Table and X = C and/or N has attracted attention as a sub-branch in materials science and technology because of their fascinating features and several research since their innovation during the 1960s.[1–6] Subject to the value of n (n = 1, 2, 3), the MAX phases M_3AX_2, M_2AX, and M_4AX_3 are indicated as 312, 211, and 413, respectively. The nanolayered ternary compounds' MAX phases provide a distinctive blend of metallic and ceramic qualities, making them sustainable for a wide range of technical implementation. They have similar properties to metals, including high conductivity, low hardness, machinability, resistance to thermal shock, and damage tolerance. Up to date, there are more than 80 MAX phase elements that have already been synthesized[7–12] and the physical characteristics are also investigated.[13–17] The M_2AX phases with M = (titanium, vanadium, chromium, niobium, tantalum, zirconium, hafnium), A = (aluminum, sulfur, Tn, arsenic, indium, gallium), and X = (nitrogen, carbon) are extensively studied conceptually and experimentally owing to their attractive properties, such as physical as well as optical and dynamical stability.[1–6,18–27] A large scientific community has paid continuous effort to add new MAX phases due to enormous demand and possible applicability resulting in more than 80 MAX phases that have already been synthesized from predicted 665 MAX phases. Very recent 2D MXenes attracted attention of scientists where the MAX[26] phase has been used as a precursor, which is a breakthrough in the history of 2D materials world, which especially enhances storage capacity where MXenes as an anode material in batteries.[28,29]

The widespread research exertion has been paid to study of M_2AX (211) phases,[13–21,26] but until now, very few are fully studied. There are a few reports on the M_2TlC (M = Ti, Zr, Hf) compounds; however, these are exhibited very much interesting and are technologically important properties.[30,31] Surprisingly, these substances have the smallest bulk moduli in the MAX phases that have been

conceptually or experimentally discovered so far. The phases are carried out using the density of states (DOS) at Fermi energy, which reduces with increasing the atomic number of transition materials. However, the phases are neither synthesized nor studied in detail yet.

A detail conceptual study of physical characteristics of materials is required to recommend a compound in technological applications. Among them, dynamical stability along with mechanical stability check is significant to judge if the material is suitable for practical application. Moreover, the compounds' stability at high temperatures and pressures is crucial to consider the materials as the basis of many industrial applications that can be determined easily by the thermodynamic properties.[32] For instance, in optoelectronic devices, significant energy dependence on the absorption coefficient and refractive index due to these properties is essential for the materials.[33] In addition, the reflectivity is a vital feature to recommend as coating materials to lessen solar heating.[34] Consequently, investigation of different features of M_2TlC (M = Ti, Zr, Hf) MAX phases is anticipated.

As a result, we intend to investigate the material characteristics of M_2TlC (M = Ti, Zr, Hf) MAX phases, as well as charge density mapping, Mulliken analysis, Fermi surface topology, and Vickers hardness.

II. COMPUTATIONAL METHODOLOGY

The density functional theory (DFT),[35] as embodied in the CASTEP program code,[36] was used to optimize the M_2TlC (M = Ti, Zr, Hf) unit cell and its physical attributes. The functional is used to represent the exchange–correlation potential using the Perdew–Burke–Ernzerhof (PBE) of Generalized Gradient Approximation (GGA).[37] The interaction between electron–ions potentials is preserved within Vanderbilt-type ultrasoft formulation[38] for M (Ti, Zr, Hf), Tl, and C atoms. The convergence is confirmed by changing the plane's energy cutoff to 400 eV and using the Monkhorst–Pack mesh for the 7 × 7 × 2 k-point samplings.[39] The tolerance is used for the geometry optimization for self-consistent field 5.0×10^{-7} eV/atom, maximum force on the atom 0.01 eV/Å, highest movement of atom 5×10^{-4} Å, and maximum stress 0.02 GPa. The optimization of atomic configuration is employed using Broyden–Fletcher–Goldfarb-Shenno (BFGS).[40]

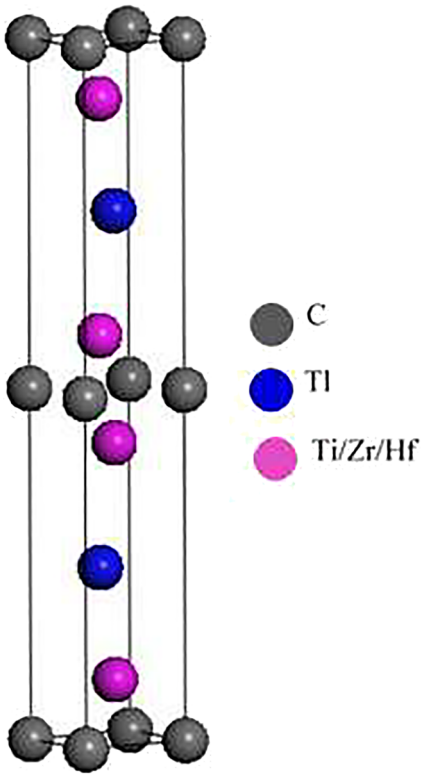

FIG. 1. The cell structure of M_2TlC (Ti_2TlC, Zr_2TlC, and Hf_2TlC).

III. RESULTS AND DISCUSSION

A. Stability of the structure

The unit cell of M_2TlC (M = Ti/Zr/Hf) is shown in Fig. 1. It crystallizes in the $P6_3/mmc$ (194) space group, which is a part of the hexagonal structure. M (Ti/Zr/Hf), A (Tl), and C's atomic positions in the unit cell are (1/3, 2/3, zM), (1/3, 2/3, 3/4), and (0, 0, 0), respectively.[30,31] The parameters of the relaxed structure at optimum conditions are shown in Table I. The obtained results show

TABLE I. Calculated lattice parameters *a*(Å), cell volume *V*(Å^3), and internal parameter z_M of the M_2TlC (Ti_2TlC, Zr_2TlC, and Hf_2TlC) compounds.

Phases	*A*	% of deviation	*c*	% of deviation	*c*/*a*	% of deviation	z_M	V	References
Ti_2TlC	3.18		14.19		4.46		0.0790	124.19	This work (GGA)
	3.17	0.03	14.20	0.01	4.48	0.02	0.0790		GGA[30,31]
	3.15	0.09	13.98	0.21	4.44	0.02			Expt.[41]
Zr_2TlC	3.39		15.16		4.47		0.0809	150.76	This work (GGA)
	3.37	0.02	15.07	0.09	4.47	0.00	0.0809		GGA[30,31]
	3.36	0.03	14.99	0.17	4.43	0.04			Expt.[41]
Hf_2TlC	3.38		14.86		4.40		0.0825	147.25	This work (GGA)
	3.37	0.01	14.85	0.01	4.41	0.01	0.0825		GGA[30,31]
	3.32	0.06	14.78	0.08	4.43	0.03			Expt.[41]

a very low deviation (within less than 0.02%) from the reported values, which proves that our calculation is well consistent and in good agreement with the previously published outcomes.[30,31,40]

Before studying different parameters, stability check of the structure, either experimentally or theoretically, is very important. We used two strategies: phonon dispersion for dynamical stability and stiffness constants for mechanical stability (C_{ij}). Ti_2TlC, Zr_2TlC, and Hf_2TlC combinations' phonon dispersion curves (PDC) are calculated using Density Functional Perturbation Theory (DFPT) along the crystal's Brillouin zone's (BZ) high symmetry orientation (density functional perturbation theory) and illustrate them in Figs. 2(a)–2(f). The PDC shows that frequencies over the range of wave vector (k) are in positive values, i.e., no negative frequency exhibits over k that indicates all studied compounds are dynamically stable. The PDC curves show distinct transverse optical (TO) and longitudinal optical (LO) components, which are accountable

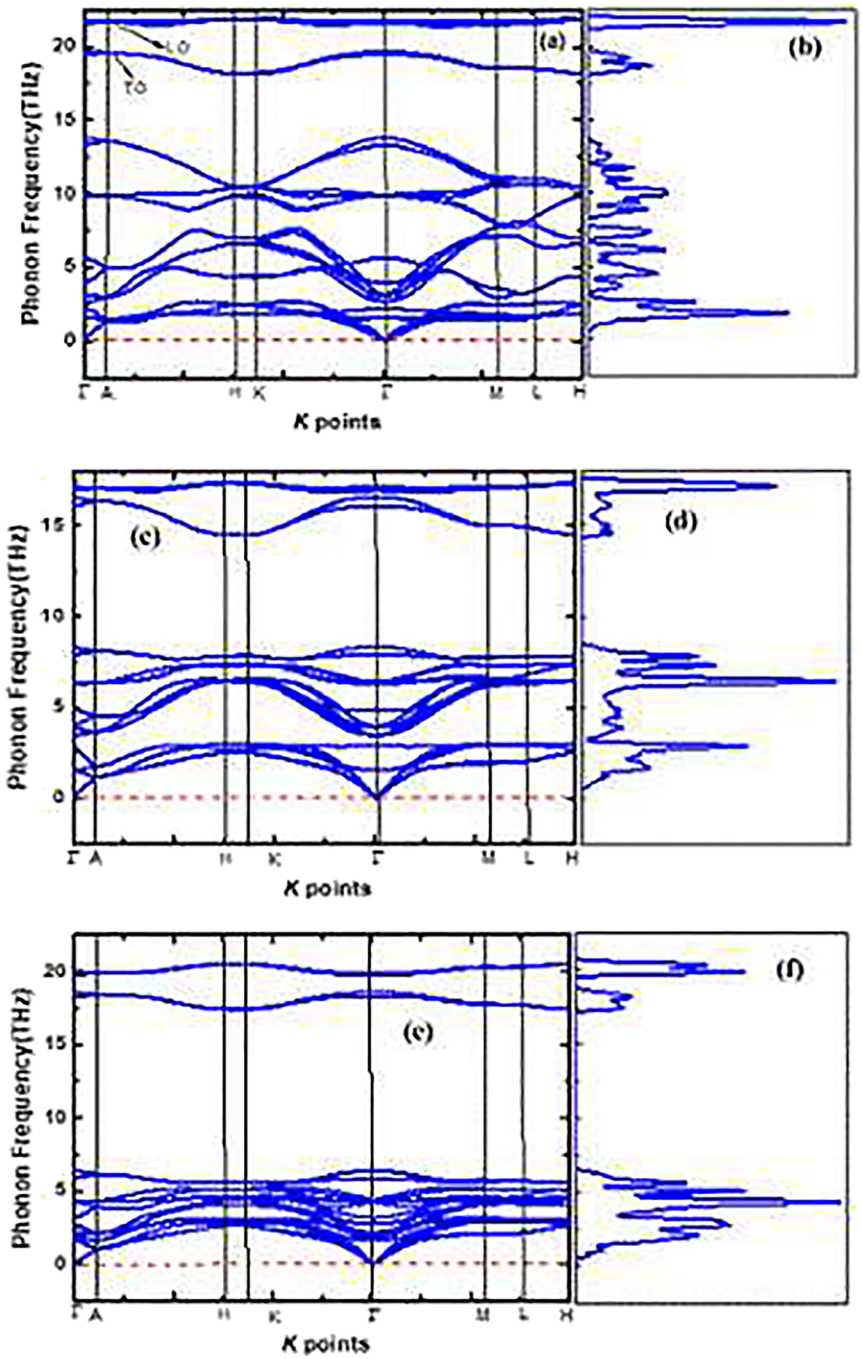

FIG. 2. The PDC and PHDOS of Ti_2TlC [(a) and (b)], Zr_2TlC [(c) and (d)], and Hf_2TlC [(e) and (f)] compounds. The red dashed line represents zero phonon frequency.

TABLE II. The calculated elastic constants, C_{ij} (GPa), various moduli [bulk B (GPa), shear, G (GPa), shear anisotropy constant, A, Young's, Y (GPa)], Pugh ratio, *G*/*B*, and Poisson ratio, and ν of MAX phases Ti_2TlC, Zr_2TlC, and Hf_2TlC compounds.

Phases	C_{11}	C_{12}	C_{13}	C_{33}	C_{44}	*A*	B	G	$Y = 9B_HG_H/(3B_H + G_H)$	G/B	MI	H_{micro}	H_{macro}	$\nu=(3B_H - Y_H)/6B_H$	References
Ti_2TlC	274	73	51	241	82	0.82	126	93	248	0.74	1.54	24	17	0.163	This
	275	73	46	223	72	0.71	123	86	210	0.70	1.71	17	15	0.210	GGA[31]
Zr_2TlC	39	69	56	204	69	0.81	115	78	211	0.68	1.67	17	13	0.207	This
	255	60	52	270	70	0.72	117	78	195	0.67	1.67	15	13	0.219	GGA[31]
Hf_2TlC	278	68	64	245	81	0.77	132	93	252	0.70	1.63	20	16	0.208	This
	278	69	62	230	71	0.68	129	86	214	0.67	1.82	16	14	0.225	GGA[31]

for the solid's optical response. The values of TO and LO are 19.74, 21.63 THz (Ti_2TlC); 16.62, 17.18 THz (Zr_2TlC); and 18.66, 19.94 THz (Hf_2TlC), respectively. The phonon DOS of Ti_2TlC, Zr_2TlC, and Hf_2TlC phases are placed next to one another for clarity in Figs. 2(b), 2(d), and 2(f), respectively, where the flat band produces noticeable peak and weak peak arises from the non-flat band.

B. Mechanical properties and hardness

Cracks are anticipated to be avoided whenever the materials are used for practical purposes. The reaction or deformation of a material to the application of a load or force is revealed by the material's mechanical characteristics. Stiffness, strength, elastic moduli, micro- and macrohardness, ductility, and toughness are important factors that define a material's mechanical qualities. The mechanical properties characterizing parameters can be used to understand the fundamental information that is necessary to choose the materials for engineering applications, including elastic moduli, stability, stiffness, brittleness, and ductility of a material. Estimated and provided in Table II are five separate elastic constants C_{ij} and polycrystalline elastic moduli, as well as any available recorded evidence[31,40] that shows the estimated elastic constants are not in decent agree with past findings. The determined C_{ij}'s meet the mechanical stability requirements for the hexagonal system:[42] $C_{11} > 0$, $C_{11} > C_{12}$, $C_{44} > 0$, $(C_{11} + C_{12})\,C_{33} - 2C_{13} > 0$. This supports the MAX phases M_2TlC's mechanical stability (Ti_2TlC, Zr_2TlC, and Hf_2TlC).

It can be seen that C_{11} indicates how much resistance is there for distortion toward the a-axis, whereas C_{33} indicates toward the c-axis. The obtained C_{11} of Ti_2TlC and Hf_2TlC is found to be higher than that of Zr_2TlC, contrary to expectations, as a result of their greater stiffness, resistance to distortion along the a-axis, and bonding strength. Ti_2TlC and Hf_2TlC compounds display significantly higher C_{44} values than Zr_2TlC, the findings in optimum shear modulus (G), as tabulated in Table II. The C_{44} values are connected to shear deformation and damage tolerant response. The C_{ij} (single-crystal elastic constants) and its corresponding compliance tensors S_{ij} ($S_{ij} = C_{ij}^{-1}$) are utilized to assess the elastic moduli *B*, *G*, *Y*, and *ν* by the equation: $Y = \frac{9B_HG_H}{(3B_H+G_H)}$ and $\upsilon = \frac{(3B_H-Y_H)}{6B_H}$.[43] The calculated findings are listed in Table II, and elastic moduli (*B*, *G*, *Y*) have been represented by Voigt–Reuss–Hill (VRH)[44,45] equations as $B_V = \frac{[2(C_{11}+C_{12})+C_{33}+4C_{13}]}{9}$ and $G_V = \frac{[C_{11}+C_{12}+2C_{33}-4C_{13}+12C_{44}+12C_{66}]}{30}$, $B_R = \frac{(C_{11}+C_{12})C_{33}-2C_{13}^2}{C_{11}+C_{12}+2C_{33}-4C_{13}}$, and $G_R = \frac{\left(\frac{5}{2}\right)[C^2C_{44}C_{66}]}{[3B_VC_{44}C_{66}+C^2(C_{44}+C_{66})]}$, $C_{66} = \frac{C_{11}-C_{12}}{2}$, Hill's value is defined by the mean of higher limit of Voigt and lower limit of Reuss as $B_H = \frac{B_R+B_V}{2}$ and $G_H = \frac{G_R+G_V}{2}$. The calculated Pugh ratios G/B for brittle materials G/B > 0.57, while its ratio in ductile materials $\nu < 0.57$. Poisson's ratios for Zr_2TlC, Ti_2TlC, and Hf_2TlC compounds were 0.207, 0.163, and 0.208, respectively, which are smaller than the value of Frantsevich's criteria (0.26),[46] showing that the examined compounds are brittle.

TABLE III. Calculated shear anisotropic A_{100}, A_{010}, and A_{001} of Ti_2TlC, Zr_2TlC, and Hf_2TlC compounds.

Phases	A_{100}	A_{010}	A_{001}
Ti_2TlC	0.78	0.82	0.64
Zr_2TlC	0.90	0.71	0.64
Hf_2TlC	0.70	0.81	0.56

We have estimated shear anisotropic factors as shown in Table III that are expressed for hexagonal solids: $A_1 = \frac{1/6(C_{11}+C_{12}+2C_{33}-4C_{13})}{C_{44}}$, $A_2 = \frac{2C_{44}}{C_{11}-C_{12}}$, and $A_3 = A_1 \cdot A_2 = \frac{1/3(C_{11}+C_{12}+2C_{33}-4C_{13})}{C_{11}-C_{12}}$ for the {100}, {010}, and {001} planes, respectively.[46] If $A_{\{100\}}$, $A_{\{010\}}$, and $A_{\{001\}}$ show unit value (one) that indicates solid is isotropic in nature otherwise exhibits anisotropic and deviation from one provides the level of anisotropy. The calculated factors indicate that the studied compounds retain anisotropy property.

Along with 2D images, a 3D contour map can be used to confirm the compounds' anisotropy. It is easier to comprehend the anisotropic behavior by using contour plots (3D) and their two-dimensional (2D) counterparts. Young's modulus, compressibility, shear modulus, and Poisson's ratio are among the variables listed in Table IV that can be utilized to evaluate the degree of anisotropy.

TABLE IV. The minimum and maximum values for the Young's, G, and Poisson's ratios of the compounds Ti_2TlC, Zr_2TlC, and Hf_2TlC.

Phases	Y_{min}	Y_{max}	Y_{max}/Y_{min}	G_{min}	G_{max}	G_{max}/G_{min}	υ_{mn}	υ_{max}	$\upsilon_{max}/\upsilon_{min}$
Ti_2TlC	211	248	1.18	87	102	1.17	0.14	0.23	1.64
Zr_2TlC	202	228	1.13	81	92	1.14	0.21	0.27	1.29
Hf_2TlC	258	292	1.13	102	121	1.19	0.20	0.28	1.4

These are computed using the ELATE open-source software and displayed in 2D and 3D contour plots, respectively.[47]

Only plots for the Ti_2TlC phase are shown in Fig. 3 since the plots for the examined compounds are almost identical. The values of Y and G are strongly anisotropic and deviate from circles in 2D perspective and spherical shapes in 3D, respectively. This is consistent with the estimated values of A in Table III and shows the phases to be strongly anisotropic. In the yz and xz planes, Y's value is anisotropic, whereas it is isotropic in the xy plane. The anisotropy factor (A) is calculated by dividing the higher and lower values of Y and G (Ref. 37) and by the degree of anisotropy (Table III). Compared to Zr_2TlC and Hf_2TlC compounds, the Ti_2TlC phase is more anisotropic.

To understand hardness of the studied compounds, we have calculated two parameters, namely micro- and macro-hardness, following the relations: $H_{micro} = \frac{(1-2\nu)E}{6(1+\nu)}$[30] and $H_{macro} = 2\left[\left(\frac{G}{B}\right)^2 G\right]^{0.585} - 3$.[33] It is seen that Ti_2TlC exhibits much higher and greater for H_{micro} (24 GPa) and H_{macro} (17 GPa) than that of Zr_2TlC (17 and 13 GPa) and Hf_2TlC (20 and 16 GPa), respectively. We can compare the hardiness of the studied compounds such a way for both hardness $Ti_2TlC > Hf_2TlC > Zr_2TlC$. The lower Poisson ratio of Ti_2TlC impacts higher hardness; however, Young modulus of Hf_2TlC is greater than Ti_2TlC. The Mulliken bond populations have been considered to calculate Vickers hardness (H_v)[13,48,49] and are presented in Table V,

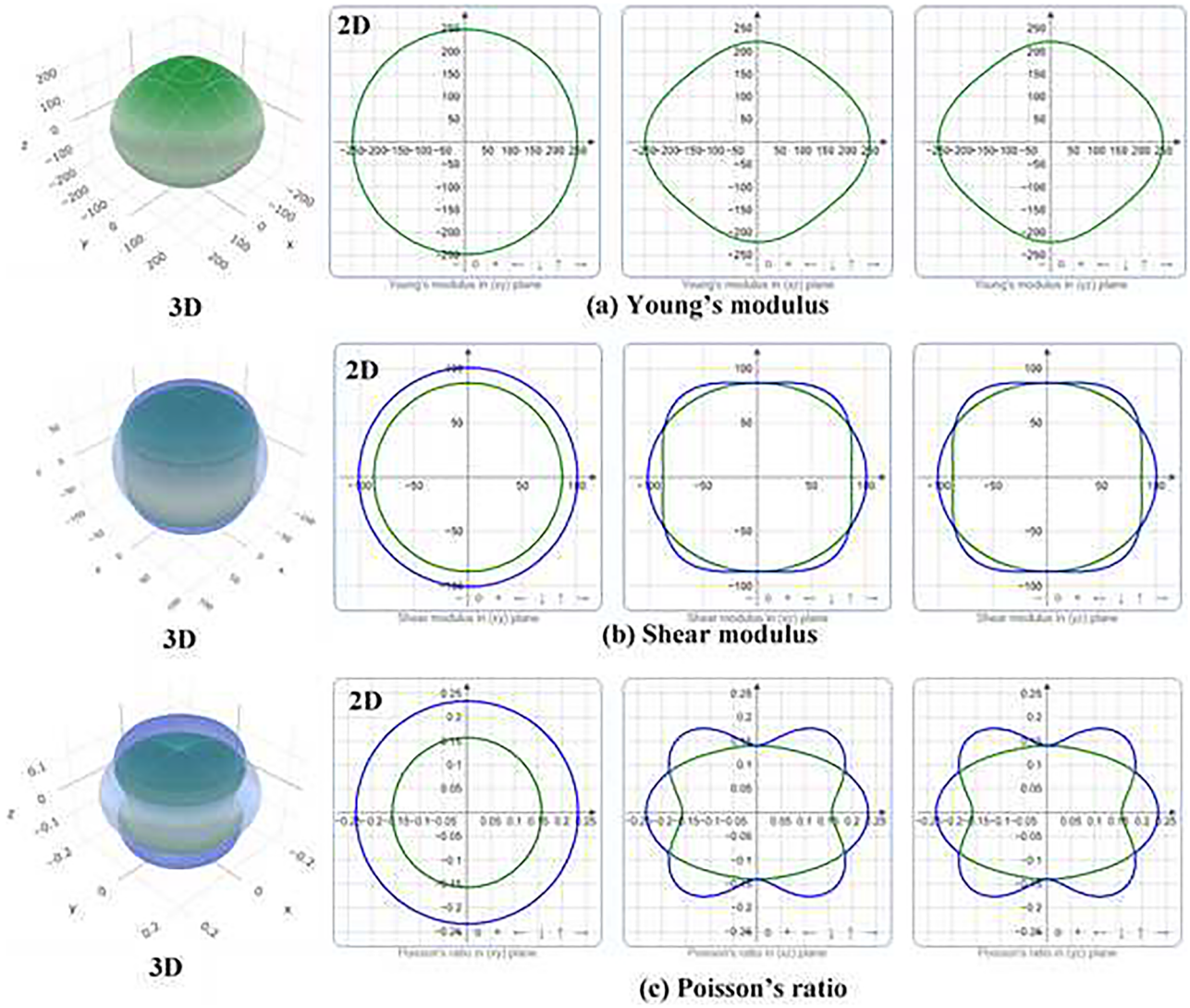

FIG. 3. Contour (3D) and two-dimensional (2D) charts of the Ti_2TlC compound's Young's modulus (Y), shear modulus (G), and Poisson's ratio (ν).

TABLE V. Calculated Mulliken populations [μ-type bond P^{μ}, bond length d^{μ} (Å) metallic population $P^{\mu'}$, bond volume $v_b{}^{\mu}$ (Å^3), and Vicker's hardness of μ-type bond $H_V{}^{\mu}$ (GPa) and H_V (GPa)] of Ti_2TlC, Zr_2TlC, and Hf_2TlC.

Phases	Bond	d^{μ}	P^{μ}	$P^{\mu'}$	$v_b{}^{\mu}$	$H_V{}^{\mu}$	H_V
Ti_2TlC	C–Ti	2.14	0.99	0.085	31.04	2.18	2.18
Zr_2TlC	C–Zr	2.30	1.00	0.077	37.69	1.61	1.61
Hf_2TlC	C–Hf	2.31	1.45	0.022	36.81	2.60	2.60

$$H_V = \left[\prod^{\mu}\left\{740\left(P^{\mu} - P^{\mu'}\right)\left(v_b^{\mu}\right)^{-5/3}\right\}^{n^{\mu}}\right]^{1/\sum n^{\mu}},$$

where P^{μ} is the Mulliken population of the μ-type bond, $P^{\mu'} = n_{free}/V$ is the metallic population, and v_b^{μ} is the bond volume of the μ-type bond. The values are determined to be 2.18, 1.61, and 2.60 GPa for the phases Ti_2TlC, Zr_2TlC, and Hf_2TlC compounds, respectively. The Hf_2TlC shows higher than Ti_2TlC and Zr_2TlC phases that are due to maximum elastic moduli. The measured hardness values correspond to the well-known MAX phase nanolaminates (in the 2–8 MPa range), including Hf_2InC (3.45 MPa) and Ta_2InC (4.12 MPa).[50]

C. Electronic properties

1. Band structure and density of states (DOS)

Ti_2TlC, Zr_2TlC, and Hf_2TlC are examples of M_2TlC compounds with high-symmetry k points. The electronic energy band structures of these compounds are depicted in Figs. 4(a)–4(c), respectively. Since the compounds' conduction bands (red colors) span the E_F line (dashed black line) and noticeably overlap the valence bands (blue lines) (black colors), no bandgap is observed, demonstrating the compounds' metallic character. Many strongly dispersive bands have been identified at and around the E_F for the phases Zr_2TlC and Hf_2TlC [Figs. 4(b) and 4(c)]. Nonetheless, a complicated hybrid band character has been observed, comprising the quasi-flat band for the Ti_2TlC combination [Fig. 4(a)] and several low dispersive bands crossing the E_F. The electrical conductivity should be lower in the c direction in contrast to the ab plane (axis), according to the energy band structure, because there is less energy dispersion there.

Understanding band structure topographies requires an awareness of both the complete and partial densities of entities. The computed total density of states (TDOS) and partial (PDOS) of the M_2TlC phases (Ti_2TlC, Zr_2TlC, and Hf_2TlC) are shown in Figs. 4(d)–4(f), where the vertically broken line denotes the Fermi level, E_F. Three sub-bands can be separated out of the valence band. The Ti-3d, C-2p [for the Ti_2TlC phase], Zr-4d, C-2p [for the Zr_2TlC

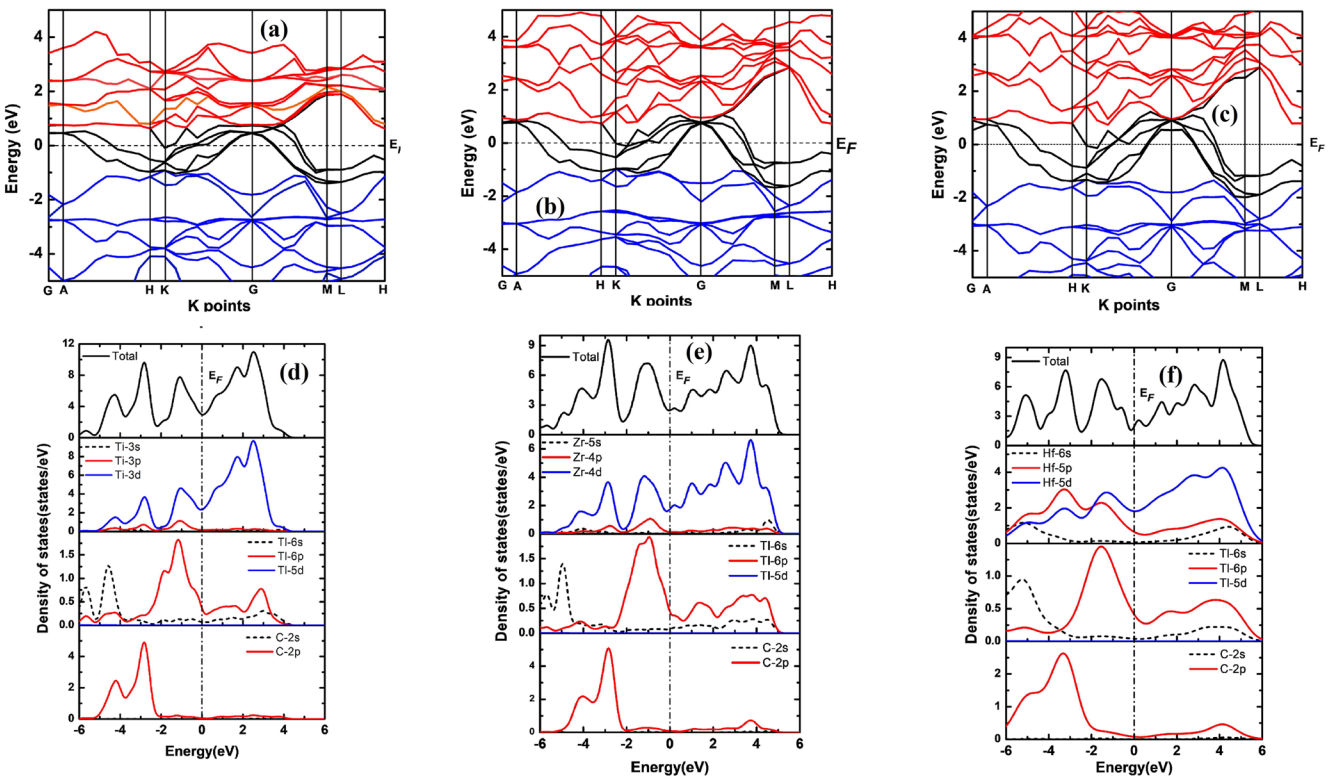

FIG. 4. Band structures of M_2TlC (a) Ti_2TlC (b) Zr_2TlC, and (c) Hf_2TlC. The total and partial density of states (DOS) of (d) Ti_2TlC, (e) Zr_2TlC, and (f) Hf_2TlC.

phase], and Hf-5p, 5d, C-2p [for the Hf_2TlC phase] states are the principal sources of the minimum energy sub-band (−6 to −2 eV).

Broad nature's middle sub-band (−2 to 0 eV) is mostly produced by the contributions due to Ti-3*p*, Ti-3*d*, Tl-6*p* [for Ti_2TlC phase], Zr-4*d*, Zr-4*p*, Tl-6*p* [for Zr_2TlC phase], Hf-5*p*, Hf-5*d*, Tl-6*p* [for Hf_2TlC phase]. The upper sub-band (0 to +6 eV) is formed by the aid of orbitals due to Ti-3*d*, Tl-6*s*, 6*p* [for Ti_2TlC phase], Zr-4*d*, Tl-6*s*, 6*p* [for Zr_2TlC phase], and Hf-6*s*, 5*p*, 5*d*, Tl-6*s*, 6*p* [for Hf_2TlC phase]. The sub-band crossing the E_F [black colors in Figs. 3(a)–3(c)] resulted mainly from Ti-3*d*, Zr-4*d*, Hf-5*p*, 5*d*, and Tl-6*p* electronic orbitals that are contributed strongly in the electronic conduction and significantly affect the physical properties of the phases. The value of DOS at E_F estimates is observed to be 3.0, 2.55, and 2.09 states/eV [Figs. 4(d)–4(f)] for Ti_2TlC, Zr_2TlC, and Hf_2TlC phases, respectively.

Six bands are firmly mixed and cross the E_F during the phase Hf_2TlC; however, four bands have crossed the E_F for Ti_2TlC and Zr_2TlC. Therefore, maximum findings of Vickers hardness are predicted for Ti_2TlC and Zr_2TlC phases compared with Hf_2TlC phase.

2. Mulliken populations study

The Mulliken atomic population (MAP) analyzes the EVC (Effective Valence Charge), and their formalism is described elsewhere.[17] The effective valence charge in a crystal refers to the distinction from the formal ionic charge and the Mulliken charge. Whether the bonds are ionic or covalent is shown by the value of EVC. When the value of EVC is zero (positive), the bond is ideal ionic in nature; nevertheless, when it deviates from zero, it displays the level of covalency. The computed EVC is shown in Table VI, which shows there is significant covalency in chemical bonding within the investigated compounds.[16,48,50]

The findings of the binary output program bond overlap population (BOP) are interpreted—(i) zero: the electronic populations of two atoms interact insignificantly; hence, the hardness calculation is omitted; (ii) positive: atoms near one another form bonds; and (iii) negative: atoms near one another form anti-bonds. Bonds with a maximum BOP value have a high level of covalency. The bond Hf–C in the compounds under study has the highest covalency

TABLE VI. Mulliken atomic populations of Ti_2TlC, Zr_2TlC, and Hf_2TlC compounds.

		Mulliken atomic population					
Phases	Atoms	*s*	*p*	*d*	Total	Charge (e)	EVC (e)
Ti_2TlC	C	1.47	3.29	0.00	4.76	−0.76	4.76
	Ti	2.22	6.72	2.64	11.59	0.41	11.59
	Tl	1.14	1.89	10.02	13.06	−0.06	13.06
Zr_2TlC	C	1.48	3.31	0.00	4.80	−0.80	4.80
	Zr	2.26	6.61	2.67	11.54	0.46	11.54
	Tl	1.19	1.90	10.02	13.12	−0.12	13.12
Hf_2TlC	C	1.54	3.35	0.00	4.89	−0.89	4.89
	Hf	0.46	0.44	2.76	3.66	0.34	3.66
	Tl	0.79	1.98	10.02	12.79	0.21	12.79

of all the bonds. Additionally, the Hf_2TlC has a stronger overall bond than Ti_2TlC and Zr_2TlC. As shown in Table V, it is therefore expected that this compound's hardness value is higher than that of the other. The well-known atomic population analysis can also be used to understand how charges move between atoms. For instance, in Ti_2TlC, charge transfers with values of 0.76 and 0.06*e*, respectively, from Ti to C and Tl. There are more compounds with comparable phase that show topographies.

D. Optical properties

When electromagnetic fields with the appropriate energy are applied to occupied (lower the E_F) and unoccupied stages, electronic transitions take place (above the E_F). As a result, in metals and systems of a similar kind, intra-band and inter-band contributions, having the latter arriving from the lower energy infrared (IR) portion of the spectra, account for the majority of the optical feature of the solids.

The dielectric capability is calculated using the following variables: 3 eV plasma frequencies and 0.05 eV damping.[50,51] Zr_2TlC, Ti_2TlC, and Hf_2TlC compounds' optical characteristics can be estimated using frequency-dependent dielectric function. The fictitious component $\varepsilon_2(\omega)$ of the dielectric function $\varepsilon(\omega)$ is calculated using the momentum matrix elements from the inhabited and uninhabited electronic stages and is given by[52]

$$\varepsilon_2(\omega) = \frac{2e^2\pi}{\Omega\varepsilon_0}\sum_{k,v,c}\left|\psi_k^c\middle|\boldsymbol{u}.\boldsymbol{r}\middle|\psi_k^v\right|^2\delta\left(E_k^c - E_k^v - E\right).$$

Here, ω is the light frequency, u is the vector representing the polarization of the input electric field, e is the electronic charge, ψ_k^c is the conduction band wave function at k, and ψ_k^v is valence band wave function at k, respectively. The Kramers–Kronig equation, which links the real and imaginary parts, may be used to compute the dielectric function's (ε_1) real portion.

Ti_2TlC, Zr_2TlC, and Hf_2TlC have had their optical characteristics estimated for photon energies between polarization vectors of the electric field up to 20 eV between [100] and [001]. An observation is made where optical spectra to these polarization directions are comparable and nearly identical. As a result, data along [100] direction are provided in Figs. 5(a)–5(h). The frequency-dependent dielectric function $\varepsilon(\omega) = \varepsilon_1(\omega) + i\varepsilon_2(\omega)$ is used to evaluate the optical properties of the substances under investigation. The transition matrix components in between inhabited and uninhabited electronic stages are used to investigate the fictitious portion of the dielectric function, ε_2, as illustrated as[53]

$$\varepsilon_2(\omega) = \frac{2e^2\pi}{\Omega\varepsilon_0}\sum_{k,v,c}\left|\psi_k^c\middle|\boldsymbol{u}.\boldsymbol{r}\middle|\psi_k^v\right|^2\delta\left(E_k^c - E_k^v - E\right).$$

The variables indicated in the aforementioned equation have conventional meanings. The Kramers–Kronig equation, which connects the actual component for the fictional part, can be employed to calculate the actual part of the dielectric function (ε_1).

Figure 5(a) illustrates the actual portion of the dielectric function, ε_1, for the phases Ti_2TlC, Zr_2TlC, and Hf_2TlC. The optical characteristics of the materials have been greatly influenced by the intra-band transition of electrons, which mostly affects the infrared spectrum's low energy area. The intra-band transition of electrons

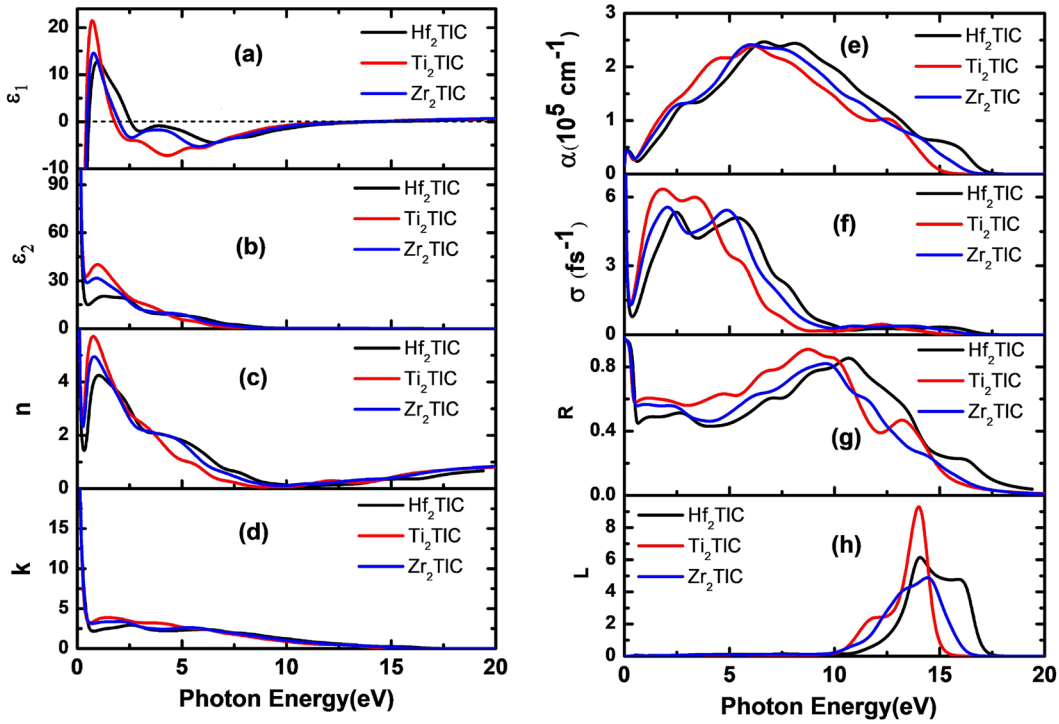

FIG. 5. Dielectric function energy dependency of (a) real part, (b) imaginary part, (c) refractive index, (d) extinction coefficient (left panel) and (e) absorption coefficient, (f) photoconductivity, (g) reflectivity, (h) loss function (right panel) of the Ti_2TlC, Zr_2TlC, and Hf_2TlC compounds for [100] direction, respectively.

causes the minimum energy peaks, which are measured to be at 0.72, 0.76, and 0.96 eV in the ε_1 curves for the Ti_2TlC, Zr_2TlC, and Hf_2TlC phases, respectively. For the materials that suggest a Drude-like behavior, the (ε_1) exhibits higher negative values, which correlates with our discussion in Sec. III C. Figure 5(b) shows the compounds' hypothetical portion, or ε_2. For the compounds Ti_2TlC, Zr_2TlC, and Hf_2TlC, respectively, the ε_1 depicts zero value from below at ~14.0, 14.5, and 13.8 eV [Fig. 5(a)], and the ε_2 approaches zero from above at ~9.96, 9.93, and 10.75 eV [Fig. 5(b)], further stating the metallic nature of the studied phases.

Figure 5 depicts the phases' computed frequency-dependent refractive index and extinction coefficient [(c) and (d)]. In the design of optoelectronic components, a material's high value of n is crucial. The primary peaks for the phases Ti_2TlC, Zr_2TlC, and Hf_2TlC, respectively, are determined to be at 0.76, 0.80, and 0.96 eV for the static values of $n(0)$, which are determined to be 20.8, 20.87, and 19.8. The relationship between the extinction and absorption coefficients is given by $k(\alpha = 4\pi k/\lambda)$. For Ti_2TlC, Zr_2TlC, and $H_{f2}TlC$, the sharp peaks were found at 1.45, 2.0, and 2.5 eV, respectively. The intra-band transitions of electrons define these peaks [Fig. 5(d)].

The energy that the electron must absorb to excite as a result of light passing through the materials is represented by the absorption coefficient. A calculation of the absorption coefficient (α) energy dependence is shown in Fig. 5(e). In the ultraviolet (UV) region, the value is strong, whereas it is weak in the IR (infrared) spectrum. The value increases steadily as photon energy rises in the direction of the UV area, peaking at 6.1, 5.9, and 6.6 eV for the compounds Ti_2TlC, Zr_2TlC, and Hf_2TlC, respectively. The fact that it has a high value throughout a huge energy range implies which might be employed in optoelectronic equipment that function in the visible and ultraviolet light spectra. Because the studied compounds are metallic, their photoconductivity begins at zero photon energy [see Fig. 5(f)].

The Ti_2TlC substance has maximum photo-conductivity at 1.81 eV, while the maxima for other compounds were 2.02 eV (Zr_2TlC) and 2.45 eV, respectively (Hf_2TlC). The compounds' photon energy-dependent reflectivity (R) spectra are shown in Fig. 5(g). As can be observed, the value of R starts out at 97% for all phases and increases to high values of 92%, 82%, and 86% for the compounds Ti_2TlC, Zr_2TlC, and Hf_2TlC, respectively, at 8.76, 9.6, and 10.7 eV. A compound with a reflectivity of 44% in the visible light band is reported to be able to reduce solar heating, according to sources.[54] The reflectivity is always over 44% for the phases Ti_2TlC (11.67 eV), Zr_2TlC (12.44 eV), and Hf_2TlC (13.8 eV) and beyond that they are not maintained, which is an interesting observation. The results of R indicate that the visible (1.7–3.3 eV) and IR (1.24 meV–1.7 eV) regions cover energy over 44% up to 12.0 eV. The studied compounds may therefore be a strong candidate for use as a covering material to lessen solar heating. The reflectance spectra of all phases strategy are zero when the input photon energy is about 20 eV.

The loss spectrum (L), which may also be interpreted using the dielectric function, is defined as the amount of energy lost by the photon during light transmission through the materials. Figure 5(h)

depicts the estimated values of L for each phase. Up to 10 eV, none of the examined chemicals exhibit any loss. In the 14–14.5 eV energy range, the loss peaks were discovered.

The peaks are more pronounced in the energy region between 0 and 1 where the dielectric function occurs. The plasma frequency, ω_P, which is determined to be at 14.0, 14.0, and 14.5 eV for the substances Ti_2TlC, Zr_2TlC, and Hf_2TlC, respectively, is linked to the loss peaks.

IV. CONCLUSIONS

The thermal and optical feature, electronic charge density, Mulliken bond overlap population, Vickers' hardness, and dynamic stability of 211 MAX phases M_2TlC (M = Ti, Zr, Hf) were investigated using first-principles pseudopotential simulations. To evaluate the accuracy of our computations, the compounds' structural, elastic, and electrical properties are reviewed. The examined lattice parameters, elastic constants, and C_{ij}, such as the polycrystalline elastic constants, were consistent with previous findings and fulfilled the traditional mechanical stability requirements. The ratios Pugh and Poisson support the brittleness of the compounds found in nature. Calculations and analyses have been done on the electronic band formation, DOS, Mulliken atomic, electron charge density locating and bond overlap populations. Since Ti_2TlC has greater elastic moduli than the other compounds tested, it exhibits a higher anisotropic index than the others. Since the valence and conduction bands overlap with E_F, no bandgaps are seen, which means the compounds are metallic. The examined phases' electronic orbitals Ti-3d, Zr-4d, Hf-5p, 5d, and Tl-6p considerably contribute to the electronic conduction that affects the physical properties. For the phases, the findings of DOS at E_F were discovered to be 3.0, 2.55, and 2.09 states per eV. According to the electronic charge mapping, strong covalent bonds are created between Ti, Zr, and Hf with Tl states, while weak covalent bonds are created between Ti, Zr, and Hf with Tl states. These strong covalent bonds are raised from the best hybridization of Ti-3d, Zr-4d, and Hf-5d with Tl-6p and C-2p electrons at the Fermi level. The phases of Ti_2TlC, Zr_2TlC, and Hf_2TlC compounds, respectively, have Vicker's hardness values of 2.18, 1.61, and 2.60 GPa, indicating a moderately hard nature to the materials. The phonon dispersion curves show no evidence of negative frequency, and as a result, the examined substances are assumed to be dynamically stable. The Debye temperatures for the phases of Ti_2TlC, Zr_2TlC, and Hf_2TlC are discovered to be 440, 369, and 334 K, respectively. The static values of n(0) are determined to be 20.8, 20.87, and 19.8, respectively, with the primary peaks for the phases Ti_2TlC, Zr_2TlC, and Hf_2TlC emerging at 0.76, 0.80, and 0.96 eV, suggesting that the materials might be utilized to create optoelectronic appliances. The values of R reveal that the visible and IR regions (1.24 meV–1.7 eV) cover above 40% of the energy up to 12.0 eV (1.7–3.3 eV). As a result, the investigated compounds represent a promising possibility for actual application as a covering material to lessen solar heating.

ACKNOWLEDGMENTS

The computing resources for this investigation were provided by the Materials Science Research Laboratory (MSRL), Department of Physics, CUET.

AUTHOR DECLARATIONS

Conflict of Interest

The authors have no conflicts to disclose.

Author Contributions

M. Sohel: Conceptualization (equal); Data curation (equal); Investigation (equal); Methodology (equal); Software (equal); Writing – original draft (equal); Writing – review & editing (equal). **M. M. Uddin**: Conceptualization (equal); Supervision (equal); Writing – original draft (equal); Writing – review & editing (equal). **M. A. Ali**: Writing – review & editing (supporting). **M. M. Hossain**: Writing – review & editing (supporting). **A. K. M. A. Islam**: Writing – review & editing (supporting). **S. H. Naqib**: Writing – review & editing (supporting).

DATA AVAILABILITY

The data that support the findings of this study are available within the article.

REFERENCES

[1] M. W. Barsoum and M. Radovic, Annu. Rev. Mater. Res. **41**, 195 (2011).
[2] V. H. Nowotny, Prog. Solid State Chem. **5**, 27 (1971).
[3] M. W. Barsoum, *MAX Phases: Properties of Machinable Ternary Carbides and Nitrides* (John Wiley & Sons, 2013).
[4] M. Naguib, G. W. Bentzel, J. Shah, J. Halim, E. N. Caspi, J. Lu, L. Hultman, and M. W. Barsoum, Mater. Res. Lett. **2**, 233 (2014).
[5] D. Horlait, S. Grasso, A. Chroneos, and W. E. Lee, Mater. Res. Lett. **4**, 137 (2016).
[6] M. W. Barsoum, Prog. Solid State Chem. **28**, 201 (2000).
[7] B. Anasori, J. Halim, J. Lu, C. A. Voigt, L. Hultman, and M. W. Barsoum, Scr. Mater. **101**, 5 (2015).
[8] E. N. Caspi, P. Chartier, F. Porcher, F. Damay, and T. Cabioc'h, Mater. Res. Lett. **3**, 100 (2015).
[9] R. Meshkian, Q. Tao, M. Dahlqvist, J. Lu, L. Hultman, and J. Rosen, Acta Mater. **125**, 476 (2017).
[10] D. Horlait, S. C. Middleburgh, A. Chroneos, and W. E. Lee, Sci. Rep. **6**, 18829 (2016).
[11] D. Horlait, S. Grasso, N. Al Nasiri, P. A. Burr, and W. E. Lee, J. Am. Ceram. Soc. **99**, 682 (2016).
[12] T. Lapauw, K. Lambrinou, T. Cabioc'h, J. Halim, J. Lu, A. Pesach, O. Rivin, O. Ozeri, E. N. Caspi, L. Hultman, P. Eklund, J. Rosén, M. W. Barsoum, and J. Vleugels, J. Eur. Ceram. Soc. **36**, 1847 (2016).
[13] F. Sultana, M. M. Uddin, M. A. Ali, M. M. Hossain, S. H. Naqib, and A. K. M. A. Islam, Results Phys. **11**, 869 (2018).
[14] M. A. Ali, M. S. Ali, and M. M. Uddin, Indian J. Pure Appl. Phys. **54**, 386 (2016). http://nopr.niscpr.res.in/handle/123456789/34407
[15] M. Roknuzzaman, M. A. Hadi, M. A. Ali, M. M. Hossain, N. Jahan, M. M. Uddin, J. A. Alarco, and K. Ostrikov, J. Alloys Compd. **727**, 616 (2017).
[16] M. A. Ali, M. M. Hossain, M. A. Hossain, M. T. Nasir, M. M. Uddin, M. Z. Hasan, A. K. M. A. Islam, and S. H. Naqib, J. Alloys Compd. **743**, 146 (2018).
[17] A. Chowdhury, M. A. Ali, M. M. Hossain, M. M. Uddin, S. H. Naqib, and A. K. M. A. Islam, Phys. Status Solidi B **255**, 1700235 (2018).
[18] M. W. Barsoum, G. Yaroschuk, and S. Tyagi, Scr. Mater. **37**, 1583 (1997).
[19] M. W. Barsoum, I. Salama, T. El-Raghy, J. Golczewski, H. J. Seifert, F. Aldinger, W. D. Porter, and H. Wang, Metall. Mater. Trans. A **33**, 2775 (2002).
[20] Z. Sun, R. Ahuja, S. Li, and J. M. Schneider, Appl. Phys. Lett. **83**, 899 (2003).
[21] Z. Sun, S. Li, R. Ahuja, and J. M. Schneider, Solid State Commun. **129**, 589 (2004).
[22] G. Hug, M. Jaouen, and M. W. Barsoum, Phys. Rev. B **71**, 024105 (2005).

[23]B. Manoun, R. P. Gulve, S. K. Saxena, S. Gupta, M. W. Barsoum, and C. S. Zha, Phys. Rev. B **73**, 024110 (2006).
[24]A. Yakoubi, L. Beldi, B. Bouhafs, M. Ferhat, and P. Ruterana, Solid State Commun. **139**, 485 (2006).
[25]A. Bouhemadou, R. Khenata, M. Kharoubi, and Y. Medkour, Solid State Commun. **146**, 175 (2008).
[26]M. F. Cover, O. Warschkow, M. M. M. Bilek, and D. R. McKenzie, J. Phys.: Condens. Matter **21**, 305403 (2009).
[27]D. Music, Z. Sun, and J. M. Schneider, Solid State Commun. **133**, 381 (2005).
[28]B. Anasori and Û. G. Gogotsi, *2D Metal Carbides and Nitrides (MXenes)* (Springer, 2019).
[29]M. Naguib and V. N. Mochalin, M. W. Barsoum, and Y. Gogotsi, Adv. Mater. **26**, 992 (2014).
[30]A. Bouhemadou, Cent. Eur. J. Phys. **7**, 753 (2009).
[31]J. A. Warner, S. K. R. Patil, S. V. Khare, and K. C. Masiulaniec, Appl. Phys. Lett. **88**, 101911 (2006).
[32]A. H. Reshak, Z. Charifi, and H. Baaziz, J. Phys.: Condens. Matter **20**, 325207 (2008).
[33]M. Xu, S. Wang, G. Yin, J. Li, Y. Zheng, L. Chen, and Y. Jia, Appl. Phys. Lett. **89**, 151908 (2006).
[34]M. C. Payne, M. P. Teter, D. C. Allan, T. A. Arias, and J. D. Joannopoulos, Rev. Mod. Phys. **64**, 1045 (1992).
[35]M. D. Segall, P. J. D. Lindan, M. J. Probert, C. J. Pickard, P. J. Hasnip, S. J. Clark, and M. C. Payne, J. Phys.: Condens. Matter **14**, 2717 (2002).
[36]S. Baroni, S. De Gironcoli, A. Dal Corso, and P. Giannozzi, Rev. Mod. Phys. **73**, 515 (2001).
[37]D. M. Ceperley and B. J. Alder, Phys. Rev. Lett. **45**, 566 (1980).
[38]D. Vanderbilt, Phys. Rev. B **41**, 7892 (1990).
[39]H. J. Monkhorst and J. D. Pack, Phys. Rev. B **13**, 5188 (1976).
[40]M. W. Barsoum, *Materials Science and Technology* (Elsevier, Amsterdam, 2006).
[41]F. Mouhat and F.-X. Coudert, Phys. Rev. B **90**, 224104 (2014).
[42]I. R. Shein and A. L. Ivanovskii, Phys. Status Solidi B **248**, 228 (2011).
[43]W. Voigt, Lehrb. Kaeltetech. **34**, 268 (1966).
[44]R. Hill, Proc. Phys. Soc., London, Sect. A **65**, 349 (1952).
[45]A. Reuß, ZAMM **9**, 49 (1929).
[46]I. N. Frantsevich and F. F. Voronov, Naukova Dumka **4**, 60 (1983).
[47]R. Gaillac, P. Pullumbi, and F.-X. Coudert, J. Phys.: Condens. Matter **28**, 275201 (2016).
[48]R. S. Mulliken, J. Chem. Phys. **23**, 1833 (1955).
[49]V. Adhikari, Z. T. Y. Liu, N. J. Szymanski, I. Khatri, D. Gall, P. Sarin, and S. V. Khare, J. Phys. Chem. Solids **120**, 197 (2018).
[50]T. Liao, J. Wang, and Y. Zhou, J. Phys.: Condens. Matter **18**, L527 (2006).
[51]D. G. Pettifor, Mater. Sci. Technol. **8**, 345 (1992).
[52]BIOVIA Material Studio, BIOVIA Materials Studio 2020 Help, 2019.
[53]P. Debye, Ann. Phys. **344**, 789 (1912).
[54]A. T. Petit and P. L. Dulong, Ann. Chem. Phys. **10**, 395 (1981).